The Astronomical Journal, 145:22 (16pp), 2013 January doi:10.1088/0004-6256/145/1/22
© 2013. The American Astronomical Society. All rights reserved. Printed in the U.S.A.

SIMULTANEOUS OBSERVATIONS OF SiO AND H_2O MASERS TOWARD KNOWN STELLAR H_2O MASER SOURCES

Jaeheon Kim[1,2,3], Se-Hyung Cho[2,4], and Sang Joon Kim[3]
[1] Yonsei University Observatory, Seongsan-ro 262, Seodaemun, Seoul 120-749, Republic of Korea; jhkim@kasi.re.kr
[2] Korean VLBI Network Yonsei Radio Astronomy Observatory, Yonsei University, Seongsan-ro 262, Seodaemun, Seoul 120-749, Republic of Korea; cho@kasi.re.kr
[3] Department of Astronomy and Space Science, Kyung Hee University, Seocheon-Dong, Giheung-Gu, Yongin, Gyeonggi-Do 446-701, Republic of Korea; sjkim1@khu.ac.kr
[4] Department of Astronomy, Yonsei University, Seongsan-ro 262, Seodaemun, Seoul 120-749, Republic of Korea
Received 2012 September 11; accepted 2012 November 4; published 2012 December 12

ABSTRACT

We present the results of simultaneous observations of SiO $v = 1$, 2, ^{29}SiO $v = 0$, $J = 1$–0, and H_2O 6_{16}–5_{23} maser lines toward 152 known stellar H_2O maser sources using the Yonsei 21 m radio telescope of the Korean VLBI Network from 2009 June to 2011 January. Both SiO and H_2O masers were detected from 62 sources with a detection rate of 40.8%. The SiO-only maser emission without H_2O maser detection was detected from 27 sources, while the H_2O-only maser without SiO maser detection was detected from 22 sources. Therefore, the overall SiO maser emission was detected from 89 sources, resulting in a detection rate of 58.6%. We have identified 70 new detections of the SiO maser emission. For both H_2O and SiO maser detected sources, the peak and integrated antenna temperatures of SiO masers are stronger than those of H_2O masers in both Mira variables and OH/IR stars and the relative intensity ratios of H_2O to SiO masers in OH/IR stars are larger than those in Mira variables. In addition, distributions of 152 observed sources were investigated in the *IRAS* two-color diagram.

Key words: circumstellar matter – masers – radio lines: stars – stars: AGB and post-AGB – stars: late-type – surveys

Online-only material: extended figure

1. INTRODUCTION

The cool luminous intermediate-mass stars (1–8 $M_\odot$) evolve from the asymptotic giant branch (AGB) stars to central stars of planetary nebulae (PNe) with significant mass loss. They are surrounded by envelopes with expansion velocities of 5–30 km s^{-1} and have high mass-loss rates of 10^{-7} to 10^{-4} $M_\odot$ yr^{-1} together with maser emission from three main species: SiO, H_2O, and OH (Habing 1996).

A number of searches for 22 GHz H_2O maser emission have been efficiently performed based on *IRAS* colors (Brand et al. 1994; Takaba et al. 1994, 2001). Catalogs of Benson et al. (1990) and the Arcetri (Comoretto et al. 1990; Valdettaro et al. 2001) provide a good data set of H_2O masers for statistical studies. Benson & Little-Marenin (1996) reported that stars with H_2O maser emission have mass-loss rates larger than 0.5×10^{-7} $M_\odot$ yr^{-1} and the low detection rate for the short-period Miras can be explained by less developed shells. Recent observational monitoring results of H_2O masers were reported by Winnberg et al. (2008) and Shintani et al. (2008). Shintani et al. (2008) indicated that the H_2O maser region has accelerated, as found by very long baseline interferometry (VLBI) observations of Imai et al. (2003) toward RT Vir. Choi et al. (2008) observed H_2O and SiO $v = 1$, 2, $J = 1$–0 masers toward the red supergiant VY CMa with the VLBI Exploration of Radio Astrometry (VERA). Their results indicated that the SiO maser spots are distributed in a ring-like structure close to the central star, while the H_2O maser spots have moved away from the central star to an outer part of the envelope, suggesting a bipolar outflow. These kinds of connected observations from SiO maser to H_2O maser regions will be important for investigating the propagation of stellar pulsation in relation to the mass-loss mechanism. A large number of H_2O maser stars also show SiO masers, while some H_2O maser stars do not show SiO masers. These different maser properties between the SiO and H_2O masers according to stars may be related to the different physical conditions and evolutionary stages of AGB stars. Collisions with hydrogen have been suggested by Cooke & Elitzur (1985) as a pumping mechanism of circumstellar H_2O masers. On the other hand, both collisional (Lockett & Elitzur 1992; Doel et al. 1995) and radiative (Bujarrabal 1994) pumpings have been suggested in the case of SiO maser emission. A scheme for the evolution of the maser emission was proposed by Lewis (1989). For these kinds of studies of complex and highly varied masers, combined studies of SiO and H_2O masers using the same telescope system will play an important role. However, even for both SiO and H_2O maser detected stars, systematic combined studies of SiO and H_2O masers have not yet been performed because homogeneous observational data are lacking. Therefore, using the Korean VLBI Network (KVN) single dish, a combined study of SiO and H_2O masers was performed for SiO and/or H_2O maser sources.

At first, we carried out simultaneous observations of SiO and H_2O masers at one epoch toward 166 known SiO and H_2O maser sources (Paper I, Kim et al. 2010). Then, we performed simultaneous observations of SiO and H_2O masers toward 83 known stellar SiO maser sources, which were not previously detected in H_2O maser emission (Paper II, Cho & Kim 2012). We detected both SiO and H_2O maser emission from 14 sources although they were not previously detected in H_2O maser emission. In this paper (Paper III), we present the results of simultaneous observations of SiO and H_2O masers toward 152 known H_2O maser sources. These are composed of 109 sources that have not been observed in the SiO maser lines before and 43 sources detected only in the 22 GHz H_2O maser emission in spite of previous SiO maser observations. Through these observations, we added the sample sources of both SiO and

Table 1
Type of Evolved Stars and Summary of Observational Results

Type of Object	Sources Surveyed	Sources Both Detected	Sources SiO-only Detected	Sources H_2O-only Detected	Sources Both Undetected
Mira variable	47	28	9	3	7
OH/IR star	41	18	15	2	6
Semi-regular variable	28	8	...	8	12
Infrared source	13	5	1	5	2
Carbon star	9	...	...	3	6
Irregular variable	8	2	...	...	6
Post-AGB star	4	...	1	1	2
Supergiant	2	1	1	...	...
Total	152	62	27	22	41

H_2O masers for statistical studies and for simultaneous KVN VLBI observations of SiO and H_2O masers. We also improved the upper limits of SiO maser emission and confirmed H_2O-only detected sources without SiO maser detections for 152 known H_2O maser sources. Continuing the results from previous observations (Papers I and II), these results may lead us to study the dynamical connection from the pulsating atmosphere to the inner circumstellar envelope through a dust formation layer in relation with mass-loss processes, including mutual relations between SiO and H_2O maser properties. Statistical analyses based on all these homogeneous data will be presented in Paper IV.

This paper is organized as follows. In Section 2, we describe the selection of sources and observations. In Section 3, observational results and comments on several individual sources are given. In Sections 4 and 5, we present the relative intensities and full line width of SiO and H_2O masers and the *IRAS* two-color diagram for observed sources, respectively. Our results are summarized in Section 6.

2. SOURCE SELECTION AND OBSERVATIONS

2.1. Source Selection

We selected 152 H_2O maser sources from the observational results of Takaba et al. (2001). Takaba et al. (2001) have detected H_2O maser emission from 179 sources among 643 objects, which were chosen from the IRAS Point Source Catalog based on *IRAS* two-color diagrams (van der Veen & Habing 1988). The selected 152 H_2O maser sources were composed of 43 sources, which were detected only in the 22 GHz H_2O maser emission in spite of SiO maser observations, and 109 sources that were not observed in the SiO maser lines. However, after completing our observations, Deguchi et al. (2010, 2012) published the survey results of SiO masers which included 21 of our objects (9 sources in Deguchi et al. 2010 and 12 sources in Deguchi et al. 2012). Therefore, 88 sources were not observed in the SiO maser lines among our 109 selected sources. Tables 1 and 2 give the list of the types and details of 152 selected sources. The selected sources are mainly Mira variables, OH/IR stars, and semi-regular variables, as shown in Table 1. In Table 2, Columns 1 and 2 give the identification number and source name, respectively. In Column 2, the object type is defined from the Simbad database (available on http://simbad.u-strasbg.fr/simbad/sim-fid). Columns 3 and 4 list the object position in right ascension (R.A.) and declination (decl.). The radial velocity of the central star, spectral type, and period are listed in Columns 5–7. Columns 8 and 9 give the value of previous observational results as the peak flux density as well as references.

2.2. Observations

We carried out simultaneous observations of SiO $v = 1, 2, J =$ 1–0 (43.122080 GHz and 42.820587 GHz), ^{29}SiO $v = 0, J =$ 1–0 (42.879916 GHz), and H_2O 6_{16}–5_{23} (22.235080 GHz) maser lines for 152 known stellar H_2O maser sources. Observations of SiO and H_2O masers occurred from 2009 June to 2010 February using the KVN Yonsei telescope. Confirmation observations have also been performed toward five sources with a bad signal-to-noise ratio (No. 13, IR Per; No. 40, AY Vir; No. 48, RZ Sco; No. 101, UV Cyg; and No. 134, IRAS 21174+1747) during 2011 January. The KVN antenna optics were designed for simultaneous observations of four bands, namely the H_2O 22 GHz and SiO 43, 86, 129 GHz bands using three low pass filters (Han et al. 2008). The signal losses due to filters were measured to be <2% (LPF 1) and <4%–6% (LPF 2) at 22/43 GHz bands. The half power beam widths and aperture efficiencies were measured to be 122″, 0.65 (at 22 GHz) and 64″, 0.67 (at 43 GHz), respectively (Lee et al. 2011). The telescope pointing was checked every 2 hr by using nearby strong SiO maser sources. We used cryogenic 22 and 43 GHz High Electron Mobility Transistor receivers with both right and left circular polarized feeds. However, as in the previous observations (Papers I and II) we only adopted the left circular polarized feed during our observations. The single side-band system noise temperatures ranged from 80 K to 290 K (at 22 GHz) and from 140 K to 350 K (at 43 GHz) depending on the weather conditions and elevations. We used a digital spectrometer with chosen total bandwidths of one 64 MHz mode for the H_2O 6_{16}–5_{23} line and three 64 MHz modes for the SiO $v = 1$, 2, and ^{29}SiO $v = 0$, $J =$ 1–0 lines in order to preserve consistency with previous observations. These bandwidths covered the range of radial velocities of 860 km s^{-1} (at 22 GHz) and 440 km s^{-1} (at 43 GHz) with velocity resolutions being 0.21 km s^{-1} (4096 channels at 22 GHz) and 0.22 km s^{-1} (2048 channels at 43 GHz), respectively.

The data were calibrated by the chopper wheel method, which corrected for atmospheric attenuation and antenna gain variations depending on the elevation, to yield an antenna temperature T_A^*. Integration time was 30–60 minutes to achieve 0.05 K at the 3σ level. The conversion factor from the antenna temperature, T_A^*, to the flux density was about 12.27 Jy K^{-1} at 22 GHz and 11.90 Jy K^{-1} at 43 GHz, respectively.

3. OBSERVATIONAL RESULTS

Table 1 summarizes the observational results according to the types of observed sources. Both SiO and H_2O maser emissions were detected from 62 sources among 152 known H_2O maser

Table 2
List of Observed Sources

No.	Source (Type)	R.A.(J2000) (h:m:s)	Decl.(J2000) (d:m:s)	V^* (km s^{-1})	Spectral Type	Period (days)	$S_{peak}(H_2O)$ (Jy)	$S_{peak}(SiO)$ (Jy)
(1)	(2)	(3)	(4)	(5)	(6)	(7)	(8)	(9)
1	V641 Cas (sr*)	00 09 26.34	+63 57 14.1	−25.7[9]	M0	...	20.8[4]	...
2	TY Cas (Mi*)	00 36 59.42	+63 08 01.7	−59.0[7]	M6	648.42	1.7[2]	7.0[a]
3	V656 Cas (Mi*)	02 35 44.67	+65 08 58.7	12.7[7]	M8	...	4.9[15]	<6.0[g]
4	YY Ari (sr*)	02 43 16.48	+22 03 34.7	−39.0[7]	M8−M9	184.00	16.0[1]	...
5	RU Ari (Mi*)	02 44 45.50	+12 19 03.0	20.0[7]	M7−M10	353.50	54.0[1]	2.4[a]
6	UZ Ari (sr*)	03 01 34.72	+21 48 12.2	−34.0[7]	M8(III)	163.00	2.5[2]	<9.4[o]
7	IO Per (SG)	03 06 47.32	+55 43 59.5	−30.0[7]	M3Iab	...	24.3[15]	...
8	GH Per (sr*)	03 13 13.71	+55 42 12.3	...	M6(III)	440.00	21.2[4]	...
9	ET Eri (sr*)	03 31 03.92	−15 24 52.2	−4.6[6]	M6(III)	...	10.0[2]	...
10	IRAS 03385+5927 (C*)	03 42 41.10	+59 37 02.0	−74.7[2]	C	...	31.1[4]	...
11	TZ Tau (Mi*)	04 02 45.67	+16 40 33.4	...	M9	269.00	4.2[2]	<9.0[g]
12	V394 Per (Ir*)	04 09 36.97	+33 29 37.4	7.0[7]	M8	...	11.4[6]	...
13	IR Per (sr*)	04 20 03.16	+41 03 50.1	−25.0[7]	M6.5	175.00	1.2[2]	...
14	V729 Tau (sr*)	04 31 07.20	+27 29 24.0	−5.0[7]	M5−M6	...	20.0[1]	...
15	BD Eri (Mi*)	04 33 44.89	+00 01 36.8	−11.0[7]	M9e	351.00	2.0[2]	<11.0[g]
16	RW Lep (sr*)	05 38 52.73	−14 02 27.2	−58.0[7]	M4−M8II	149.90	76.0[1]	<10.0[g]
17	LO Aur (Mi*)	05 57 23.94	+48 22 41.8	3.0[7]	M8−M9	490.00	11.5[2]	23.5[a]
18	V1307 Ori (pA*)	06 01 59.55	+16 30 55.7	18.0[7]	B9eq	...	2.1[19]	...
19	S Lep (sr*)	06 05 45.55	−24 11 44.1	−10.0[7]	M5−M6III	89.00	1.8[16]	<3.6[h]
20	IRAS 06319−0501 (OH*)	06 34 26.20	−05 03 38.0	−59.0[7]	...	...	7.2[2]	<0.2[c]
21	FX Mon (Mi*)	06 45 05.60	+09 02 18.5	30.0[7]	M1−M8	428.50	1.5[2]	3.2[a]
22	IRC+70074 (Mi*)	07 10 05.89	+65 56 24.9	10.4[7]	M8	459.00	1.7[2]	5.8[a]
23	TT Mon (Mi*)	07 25 40.62	−05 51 01.3	42.0[7]	M5e−M8	323.17	3.6[14]	...
24	OZ Gem (Mi*)	07 33 57.75	+30 30 37.8	7.0[7]	M9.5	...	31.4[2]	<7.0[g]
25	SS Pup (Mi*)	07 46 38.29	−26 20 35.9	83.0[7]	M6e	391.00	10.6[2]	...
26	SV Pup (Mi*)	08 17 16.65	−13 48 30.5	30.0[7]	M5e	166.52	3.2[5]	...
27	V429 Hya (sr*)	08 55 43.80	−19 13 27.6	4.0[7]	M6−M7	117.00	3.9[2]	<9.0[g]
28	V Leo (Mi*)	10 00 01.92	+21 15 44.4	−27.0[7]	M5e−M7e	273.35	16.0[17]	†<6.3[l]
29	AF Leo (sr*)	11 27 53.14	+15 08 48.6	6.0[5]	M5(II)	107.00	17.6[1]	<0.1[e]
30	AZ UMa (Ir*)	11 47 13.80	+43 28 15.9	...	M6III	...	20.0[3]	<0.2[e]
31	II Hya (sr*)	11 48 45.08	−26 44 59.2	20.0[7]	M4III	61.00	50.0[20]	...
32	S Crt (sr*)	11 52 45.10	−07 35 48.1	38.0[7]	M6e−M7e	155.00	37.6[1]	<9.0[g]
33	SV Vir (Mi*)	12 00 20.79	−10 11 04.9	−3.0[7]	M4e	295.33	12.0[1]	4.3[a]
34	Y UMa (sr*)	12 40 21.29	+55 50 47.4	16.8[6]	M7II−III:	168.00	23.0[4]	<15.1[n]
35	U CVn (Mi*)	12 47 19.61	+38 22 30.7	−30.0[9]	M7e	345.65	34.0[1]	<10.0[g]
36	T Com (Mi*)	12 58 38.90	+23 08 21.1	27.0[7]	M2:−M9e	406.00	3.9[2]	6.0[b]
37	IRC−10278 (IR)	13 09 31.28	−09 43 25.6	94.0[7]	M4−M5	206.90	7.3[10]	...
38	V CVn (Mi*)	13 19 27.77	+45 31 37.7	−2.0[9]	M4e−M6eIIIa	191.89	20.8[5]	<5.4[l]
39	T UMi (Mi*)	13 34 41.08	+73 25 53.0	1.0[7]	M4e−M6e	301.00	1.1[10]	<10.0[g]
40	AY Vir (sr*)	13 51 51.67	−03 40 34.0	−43.0[7]	M6	113.00	5.9[2]	<10.0[g]
41	TW Cen (Mi*)	13 57 43.18	−31 04 11.0	3.0[7]	M4e−M8II:	269.27	3.7[14]	2.5[a]
42	R Boo (Mi*)	14 37 11.54	+26 44 11.0	−44.0[7]	M3e−M8e	223.40	2.4[5]	<12.0[n]
43	IRC−20285 (IR)	15 22 19.06	−18 40 00.6	−2.0[7]	M7(III)	201.86	3.4[2]	<0.2[l]
44	MW Ser (Mi*)	15 28 43.70	+03 49 43.1	45.0[7]	M9(III)	...	0.7[9]	19.3[b]
45	WW Ser (Mi*)	15 32 24.84	+03 38 27.0	21.0[7]	M8e	365.80	30.2[1]	<11.0[g]
46	SW Lib (Mi*)	15 55 33.42	−12 51 05.5	−20.0[7]	M7(III)	291.80	2.7[2]	...
47	X Her (sr*)	16 02 39.17	+47 14 25.3	−89.0[1]	M6e	102.00	1.8[2]	<9.5[n]
48	RZ Sco (Mi*)	16 04 36.13	−24 06 00.6	−174.0[9]	M3e−M4e	156.60	1.6[5]	...
49	S Sco (Mi*)	16 17 40.24	−22 53 35.6	85.0[9]	M(3)e	177.92	3.2[5]	...
50	RY CrB (sr*)	16 23 05.11	+30 51 00.6	28.0[5]	M10III	90.00	0.3[9]	<0.3[e]
51	R Dra (Mi*)	16 32 40.22	+66 45 17.9	−120.0[7]	M5e−M9eIII	245.60	26.0[1]	<13.0[k]
52	RX Oph (Mi*)	16 52 48.21	+05 24 27.0	−48.0[7]	M5(III)	322.93	14.2[2]	6.1[b]
53	TU Sco (Mi*)	17 07 35.78	−31 49 29.8	−18.0[7]	M7IIe−M9	373.04	2.7[2]	...
54	V438 Oph (sr*)	17 14 39.78	+11 04 10.0	9.0[7]	M0−M7e	169.90	27.5[9]	...
55	UY Oph (Mi*)	17 16 24.84	+04 43 16.7	−63.5[4]	M7III	332.00	1.5[2]	...
56	RV Ser (Mi*)	17 17 50.48	−11 59 33.2	1.0[7]	M4IIIe−M8	269.90	17.5[15]	...
57	IRAS 17187−3750 (IR)	17 22 11.20	−37 53 13.0	−26.0[7]	...	...	9.3[7]	<7.0[i]
58	AH Oph (Mi*)	17 25 35.86	−03 04 00.8	53.0[7]	M7	353.20	35.3[2]	...
59	IRAS 17230+0113 (OH*)	17 25 36.51	+01 11 06.0	−25.0[7]	...	730.00	3.5[2]	1.8[a]
60	V2296 Oph (Mi*)	17 28 08.31	+05 02 18.5	26.0[7]	M8:	369.00	8.0[1]	4.8[a]
61	MW Her (Mi*)	17 35 40.00	+15 35 12.2	−53.0[7]	M8−M9	449.00	43.0[2]	...
62	OH358.23+0.11 (OH*)	17 40 53.40	−30 23 09.0	−10.0[7]	...	...	41.6[2]	<9.0[g]
63	IRAS 17528+1144 (OH*)	17 55 13.71	+11 43 46.2	87.0[7]	...	...	0.1[9]	<0.6[b]
64	WY Her (Mi*)	18 00 03.92	+23 35 37.2	3.0[7]	M5e−M7e	376.00	3.2[2]	3.8[b]

Table 2
(Continued)

No.	Source (Type)	R.A.(J2000) (h:m:s)	Decl.(J2000) (d:m:s)	V^* (km s^{-1})	Spectral Type	Period (days)	$S_{peak}(H_2O)$ (Jy)	$S_{peak}(SiO)$ (Jy)
(1)	(2)	(3)	(4)	(5)	(6)	(7)	(8)	(9)
65	IRC+10346 (IR)	18 01 49.60	+08 27 01.0	16.0[7]	M5(III)	98.77	0.3[9]	...
66	IRC−10395 (IR)	18 06 42.88	−08 13 12.0	20.0[7]	M8	150.59	5.0[2]	...
67	OH10.4+0.04 (OH*)	18 08 38.00	−19 54 54.0	64.0[7]	F3	...	2.2[2]	...
68	IRC+30330 (IR)	18 14 26.50	+30 11 41.0	...	M5(III)	...	1.0[2]	...
69	IRAS 18139−1811 (OH*)	18 16 54.90	−18 10 44.0	34.3[2]	...	...	4.6[2]	...
70	IRAS 18156−0653 (C*)	18 18 18.80	−06 51 52.0	23.7[2]	C9,4e	730.00	20.0[3]	...
71	TU Lyr (Ir*)	18 20 30.28	+31 45 21.3	...	M6e	...	2.7[2]	...
72	V2090 Oph (Ir*)	18 23 52.21	+03 37 22.8	−30.3[7]	M6:−M9	220.80	1.8[2]	...
73	IRAS 18231+0855 (OH*)	18 25 33.36	+08 56 47.3	−8.0[7]	...	...	1.4[9]	0.9[b]
74	UY Sct (sr*)	18 27 36.53	−12 27 58.9	25.5[5]	M4Ia−Iab	740.00	10.5[2]	...
75	IRC−10425 (IR)	18 28 04.80	−13 03 39.0	39.5[5]	M5(III)	300.62	17.8[2]	...
76	V2571 Oph (sr*)	18 29 34.58	+03 28 11.7	−36.0[7]	...	206.06	1.7[9]	...
77	V445 Sct (pA*)	18 30 30.62	−14 28 55.8	61.4[7]	K1−K4	890.00	88.1[12]	<18.1[m]
78	OH24.7−0.1 (OH*)	18 36 45.88	−07 18 18.0	86.2[7]	...	225.00	2.2[2]	...
79	IRAS 18375+0510 (OH*)	18 39 59.65	+05 13 14.2	75.0[7]	...	...	1.0[9]	...
80	IRC+00364 (IR)	18 42 08.43	−02 45 15.4	50.0[7]	M7	...	10.4[2]	...
81	V3952 Sgr (Mi*)	18 45 51.33	−17 17 59.4	−1.0[3]	M9(III)	476.60	10.7[2]	...
82	OH40.1+2.4 (OH*)	18 55 57.00	+07 30 32.0	47.1[3]	...	...	0.1[9]	...
83	IRAS 18549+0905 (OH*)	18 57 20.82	+09 09 40.9	19.0[7]	...	...	8.8[9]	...
84	IRAS 18556+0811 (OH*)	18 58 04.23	+08 15 30.8	28.0[7]	...	...	1.0[9]	<6.6[h]
85	EU Aql (Mi*)	18 58 23.76	+16 46 54.8	74.0[7]	M9	321.00	2.5[8]	...
86	IRAS 18567+0003 (OH*)	18 59 21.17	+00 07 26.4	48.0[7]	...	...	0.2[9]	...
87	OH43.9+1.2 (OH*)	19 06 43.00	+10 14 32.0	50.0[7]	...	...	0.3[9]	...
88	IRAS 19061+1041 (OH*)	19 08 31.20	+10 46 47.4	37.0[7]	...	...	3.0[2]	...
89	OH43.8+0.5 (OH*)	19 09 32.00	+09 51 49.0	9.0[7]	...	...	0.7[9]	...
90	IRAS 19075+0921 (C*)	19 09 57.15	+09 26 52.2	12.3[6]	...	...	1.5[2]	...
91	IRAS 19083+0851 (OH*)	19 10 47.33	+08 56 22.9	56.8[6]	...	...	5.5[2]	...
92	IRAS 19087+0323 (OH*)	19 11 17.01	+03 28 24.4	22.0[7]	...	344.35	1.7[9]	...
93	RU Lyr (Mi*)	19 12 21.26	+41 18 13.3	15.0[7]	M6e:−M8e	371.84	3.7[14]	<9.0[g]
94	IRAS 19110+1045 (IR)	19 13 22.06	+10 50 53.4	54.0[7]	...	...	21.5[2]	...
95	IRAS 19134+2131 (pA*)	19 15 35.36	+21 36 33.1	−66.0[7]	...	...	0.3[9]	<0.2[d]
96	IRAS 19161+2343 (OH*)	19 18 14.67	+23 49 27.9	30.0[7]	M	...	1.0[9]	...
97	IRAS 19186+0315 (OH*)	19 21 11.70	+03 20 57.9	−22.0[7]	M	454.99	9.4[9]	0.8[b]
98	YZ Dra (Mi*)	19 23 45.18	+71 41 13.7	15.0[7]	M8e	347.60	190.0[1]	8.8[b]
99	IRAS 19229+1708 (OH*)	19 25 12.50	+17 14 49.5	42.0[7]	M4:IE	...	7.9[2]	...
100	IRC−20563 (IR)	19 27 40.69	−17 15 59.2	−37.0[6]	M8(III)	139.13	19.2[2]	...
101	UV Cyg (sr*)	19 31 13.28	+43 38 13.6	...	M6−M8	135.50	2.9[2]	...
102	IRAS 19303+1553 (OH*)	19 32 35.88	+15 59 41.1	6.0[3]	...	...	1.3[9]	...
103	V1965 Cyg (Mi*)	19 34 09.87	+28 04 06.3	−12.0[2]	C	577.00	21.8[4]	...
104	V1319 Aql (Ir*)	19 36 03.49	−00 26 51.4	−24.0[7]	M8	...	15.5[6]	...
105	IRAS 19374+0550 (IR)	19 39 53.03	+05 57 53.2	−17.2[7]	...	...	4.9[2]	<7.5[g]
106	IRAS 19387+1527 (OH*)	19 41 03.14	+15 34 19.3	64.0[7]	...	...	2.4[2]	...
107	IRAS 19422+3506 (OH*)	19 44 07.00	+35 14 08.2	−49.0[7]	M7.5III	...	2.0[2]	...
108	IRAS 19456+1927 (OH*)	19 47 49.68	+19 35 23.0	−69.0[7]	...	...	0.9[9]	...
109	IRAS 19455+0920 (C*)	19 47 56.30	+09 28 10.0	49.3[2]	...	...	28.4[4]	...
110	OH59.2−1.8 (OH*)	19 48 09.40	+22 19 31.0	−36.0[8]	...	...	0.4[13]	...
111	IRAS 19495+0835 (OH*)	19 51 57.71	+08 42 54.6	45.0[7]	...	...	2.8[2]	...
112	IRAS 19499+2141 (OH*)	19 52 07.43	+21 49 28.4	2.4[3]	M8:III:	...	2.2[9]	...
113	IRAS 19522+1935 (OH*)	19 54 29.00	+19 43 44.0	66.0[7]	...	...	1.3[9]	11.0[b]
114	IRAS 19566+3423 (OH*)	19 58 32.28	+34 31 33.7	−43.7[3]	...	...	1.3[2]	...
115	V718 Cyg (sr*)	20 03 05.12	+30 20 12.9	21.1[7]	M0−M5	264.00	12.0[3]	...
116	V719 Cyg (OH*)	20 03 38.49	+30 28 09.4	17.3[7]	M4e	...	21.6[2]	...
117	IRAS 20097+1107 (OH*)	20 12 09.17	+11 16 51.6	−13.0[7]	...	...	1.9[9]	2.5[b]
118	IRC−10530 (IR)	20 12 14.27	−11 12 19.5	...	M7(III)	...	3.6[2]	...
119	AC Cyg (sr*)	20 12 49.80	+49 27 03.1	−42.0[7]	M7−M8	142.00	4.8[5]	...
120	V557 Cyg (Mi*)	20 12 57.97	+32 14 56.3	53.3[9]	M7−M9	382.00	14.5[2]	1.1[a]
121	IRAS 20171+2732 (OH*)	20 19 11.08	+27 42 11.9	46.9[3]	...	...	0.7[9]	<8.0[g]
122	IRAS 20246+2813 (OH*)	20 26 46.61	+28 23 58.7	18.0[7]	...	...	1.1[9]	<8.0[g]
123	IRAS 20311+4222 (C*)	20 32 55.00	+42 32 56.0	24.9[2]	C	...	24.2[4]	...
124	V778 Cyg (C*)	20 36 07.37	+60 05 25.9	−17.0[7]	C4,5J(N)	...	74.0[4]	<0.4[j]
125	V2319 Cyg (OH*)	20 38 19.82	+34 12 20.7	14.3[3]	...	...	1.9[2]	...
126	IRAS 20403+3700 (OH*)	20 42 18.49	+37 11 41.0	−51.0[7]	...	...	6.0[3]	...
127	V Aqr (sr*)	20 46 49.36	+02 26 15.2	−44.0[7]	M6e	249.07	1.3[16]	...
128	IRAS 20482+3325 (OH*)	20 50 18.00	+33 36 33.2	47.0[7]	...	401.00	0.7[9]	...

Table 2
(Continued)

No.	Source (Type)	R.A.(J2000) (h:m:s)	Decl.(J2000) (d:m:s)	V^* (km s^{-1})	Spectral Type	Period (days)	$S_{peak}(H_2O)$ (Jy)	$S_{peak}(SiO)$ (Jy)
(1)	(2)	(3)	(4)	(5)	(6)	(7)	(8)	(9)
129	OH83.42−0.89 (OH*)	20 50 58.60	+42 48 11.0	−39.0[7]	...	...	3.1[2]	...
130	U Equ (pA*)	20 57 16.28	+02 58 44.6	−75.0[7]	M	...	3.6[11]	<0.5[b]
131	V1899 Cyg (sr*)	21 04 14.52	+53 21 04.8	...	C8,3e	...	33.1[4]	...
132	RX Aqr (Ir*)	21 12 46.39	−14 23 33.0	...	M6III	537.78	14.2[2]	...
133	IRAS 21120+0736 (OH*)	21 14 29.57	+07 48 33.7	29.0[7]	M	730.00	8.0[1]	7.8[a]
134	IRAS 21174+1747 (OH*)	21 19 44.94	+18 00 29.8	−74.0[7]	M	730.00	2.5[9]	...
135	GH Cep (Mi*)	21 20 04.40	+77 50 44.0	36.0[4]	M3(III)	331.00	3.0[3]	...
136	IRAS 21305+2118 (OH*)	21 32 53.70	+21 32 00.0	−43.0[7]	...	...	25.5[4]	...
137	AM Cep (Mi*)	21 41 27.08	+76 23 11.3	−50.0[7]	M8(III)	333.00	59.5[6]	...
138	TW Peg (sr*)	22 03 59.51	+28 20 54.2	−10.0[7]	M6−M8	929.30	71.4[18]	<7.0[g]
139	IRC+60342 (Ir*)	22 06 29.90	+59 29 28.0	−2.8[9]	M4I	435.00	1.2[2]	<0.2[a]
140	CU Cep (Mi*)	22 11 31.88	+57 02 17.4	−51.0[7]	M4−M6	700.00	4.8[5]	...
141	V384 Cep (C*)	22 25 54.81	+60 20 42.4	−6.0[2]	C	698.00	27.6[4]	...
142	IRC+50434 (Ir*)	22 29 53.50	+45 50 10.0	60.0[7]	M8(III)	...	43.3[15]	...
143	MP Peg (Mi*)	22 42 47.13	+11 00 53.9	−103.0[7]	M7−M8	239.00	1.8[9]	...
144	V386 Cep (sr*)	22 53 12.33	+61 17 00.4	−49.2[7]	M3−M6II:S	...	13.9[2]	...
145	LL Peg (Mi*)	23 19 12.39	+17 11 35.4	−31.0[6]	M	696.00	58.1[4]	...
146	EU And (C*)	23 19 58.89	+47 14 34.6	−30.0[7]	C4,4J:	...	32.0[1]	<0.5[j]
147	RY And (Mi*)	23 20 37.59	+39 37 14.0	−2.0[7]	M8(III)	391.20	62.0[1]	27.0[a]
148	IRAS 23279+5336 (C*)	23 30 17.98	+53 53 07.2	−32.0[2]	C	...	26.7[4]	...
149	IRC+10537 (IR)	23 33 47.07	+06 17 55.0	−20.0[7]	M7	97.58	18.7[15]	<8.0[g]
150	PZ Cas (SG)	23 44 03.29	+61 47 22.2	−43.0[7]	M2−M4Ia	925.00	50.0[1]	<3.5[f]
151	V657 Cas (Mi*)	23 52 04.92	+61 48 12.4	−21.0[7]	M8.9−M10.2	...	5.3[15]	<6.0[g]
152	RS And (sr*)	23 55 21.74	+48 38 17.7	−1.0[5]	M7−M10	136.00	2.2[16]	<7.0[g]

Notes. "Mi*" indicates a variable star of Mira Cet type, "OH*" denotes a star with an envelope of OH/IR type,"sr*" indicates a semi-regular variable star, "IR" denotes an infrared source, "C*" denotes a carbon star, "Ir*" indicates an irregular variable star, "pA*" denotes a post-AGB star (proto-PN), and "SG" indicates a supergiant.
Source type reference: SIMBAD astronomical database, CDS, Strasbourg, France.
Position reference: NASA/IPAC Infrared Science Archive.
Stellar velocity references: (1) Famaey et al. 2005; (2) Groenewegen et al. 2002; (3) Chen et al. 2001; (4) Feast & Whitelock 2000; (5) Barbier-brossat et al. 1994; (6) Le Squeren et al. 1992; (7) Benson et al. 1990; (8) Engels et al. 1984; (9) Wilson 1953.
Spectral type and period references: GCVS of Samus et al. (2011), Benson et al. (1990), AAVSO International Database.
Column 8: $S_{peak}(H_2O)$, peak flux density of H_2O ($6_{16}-5_{23}$).
Column 9: $S_{peak}(SiO)$, peak flux density of SiO ($v = 1$, $J = 1$–0); †, SiO ($v = 1$, $J = 2$–1).
H_2O references: (1) Shintani et al. 2008; (2) Takaba et al. 2001; (3) Valdettaro et al. 2001; (4) Han et al. 1998; (5) Benson & Little-Marenin 1996; (6) Comoretto et al. 1990; (7) Deguchi et al. 1989; (8) Benson & Little-Marenin 1989; (9) Lewis & Engels 1988; (10) Engels et al. 1988; (11) Zuckerman & Lo 1987; (12) Engels et al. 1986; (13) Engels et al. 1984; (14) Bowers & Hagen 1984; (15) Crocker & Hagen 1983; (16) Dickinson & Dinger 1982; (17) Kleinmann et al. 1978; (18) Dickinson 1976; (19) Schwartz & Buhl 1975; (20) Dickinson et al. 1973.
SiO references: (a) Deguchi et al. 2012; (b) Deguchi et al. 2010; (c) Deguchi et al. 2007; (d) Nakashima & Deguchi 2003; (e) Ita et al. 2001; (f) Cho et al. 1996; (g) Takaba et al. 1994; (h) Hall et al. 1990b; (i) Hall et al. 1990a; (j) Nakada et al. 1987; (k) Bujarrabal et al. 1987; (l) Nyman et al. 1986; (m) Jewell et al. 1984; (n) Spencer et al. 1981; (o) Zuckerman 1979; (p) Balister et al. 1977.

sources, at a detection rate of 40.8%. SiO-only maser emission without H_2O maser detections was detected from 27 sources, while H_2O-only maser emission without SiO maser detections was detected from 22 sources. Therefore, the total detection rate of SiO masers was 58.6% and that of H_2O masers was 55.3%, respectively. We have identified 19 new detections of SiO maser emission for 43 previous non-detection sources of SiO masers and 51 new detections of SiO masers for 88 sources of SiO masers previously not observed. The ^{29}SiO $v = 0$, $J = 1$–0 maser was detected from four stars. Different detection rates of SiO and/or H_2O masers were found based on the types of evolved stars. In 47 Mira variables, both SiO and H_2O masers were detected from 28 sources (60%), SiO-only masers from 9 sources, and H_2O-only masers from 3 sources. On the other hand, for 41 OH/IR stars, both SiO and H_2O masers were detected from 18 sources (44%), SiO-only masers from 15 sources, and H_2O-only masers from 2 sources. In the case of semi-regular variables, 8 of 28 surveyed sources emitted both SiO and H_2O masers (29%), and the detection rate of the H_2O maser (57%) was much higher than that of the SiO maser (29%) with the most numerous H_2O-only maser detections. Among the 43 selected sources that were only detected in the 22 GHz H_2O maser emission before in spite of SiO maser observations, both SiO and H_2O masers were detected from 13 sources, SiO-only masers from 6 sources, H_2O-only masers from 11 sources, and both non-detections from 13 sources. These results demonstrate that both maser detectabilities are strongly dependent upon stellar phases, including telescope sensitivities, as shown in Paper II. Tables 3 and 4 present the observational results of both SiO and H_2O detected sources. In Table 3, the identification number and the source name are given in Columns 1 and 2. Columns 3–6 list the peak antenna temperatures of each maser line of SiO $v = 1$, 2, $J = 1$–0, ^{29}SiO $v = 0$, $J = 1$–0, and H_2O 6_{16}–5_{23}. Columns 7–10 list the peak velocities with respect to the local standard of rest (LSR) at which each occurs. The date of observations with the corresponding phase of the optical light curve (0.0 = maximum light) are listed in Column 11. The

Table 3
Peak Antenna Temperatures and Velocities of both SiO ($J = 1$–0) and H_2O Detected Sources

No.	Source	T_A^*(peak) (K)				V_{LSR}(peak) (km s^{-1})				Date(Phase)
		^{28}SiO		^{29}SiO	H_2O	^{28}SiO		^{29}SiO	H_2O	(yymmdd)
		$v = 1$	$v = 2$	$v = 0$		$v = 1$	$v = 2$	$v = 0$		
(1)	(2)	(3)	(4)	(5)	(6)	(7)	(8)	(9)	(10)	(11)
13	IR Per	0.21	0.21	0.08	<0.07	−22.3	−28.7	−27.9	...	091203
		0.14	0.10	<0.05	0.22	−28.0	−23.3	...	−18.6	110120
15	BD Eri	0.62	0.38	<0.07	0.48	−7.3	−7.3	...	−9.7	091202(0.99)
16	RW Lep	0.32	0.80	<0.07	1.15	−57.7	−59.6	...	−59.8	100111
17	LO Aur	0.60	0.42	...	0.28	0.4	2.7	...	4.6	090615(0.71)
22	IRC+70074	0.58	0.98	...	0.18	9.1	10.4	...	8.9	090615
23	TT Mon	0.17	<0.10	...	0.52	39.2	...	...	43.0	091113(0.55)
24	OZ Gem	2.44	2.16	...	0.48, 0.40	4.3	4.5	...	0.2, 14.7	090716
25	SS Pup	1.25	1.27	...	0.40	81.8	81.0	...	85.3	091113(0.99)
28	V Leo	0.16	<0.11	...	2.06	−24.4	...	...	−26.8	090610(0.93)
35	U CVn	0.48	<0.12	...	0.47	−26.7	...	...	−22.9	091113(0.72)
36	T Com	0.84	0.47	...	0.11	28.3	30.8	...	28.0	091110(0.78)
41	TW Cen	0.43	0.23	0.17	0.33	−0.8	−0.8	0.3	3.8	091111(0.80)
42	R Boo	0.60	0.28	...	0.15	−45.0	−44.4	...	−43.2	091110(0.47)
46	SW Lib	0.27	0.14	<0.05	0.18	−22.9	−22.0	...	−19.2	100116(0.56)
51	R Dra	0.48	0.52	...	0.44	−121.7	−115.2	...	−121.4	091110(0.11)
53	TU Sco	1.03	0.50	<0.11	0.41	−14.3	−13.8	...	−12.7	100117(0.73)
54	V438 Oph	<0.09	0.13	...	0.13	...	9.8	...	8.9	091110
55	UY Oph	0.32	0.33	<0.06	0.12	−66.0	−63.1	...	−63.5	100119(0.43)
56	RV Ser	0.34	0.37	<0.07	2.09	0.7	1.3	...	2.1	100124(0.47)
57	IRAS 17187−3750	1.39	0.54	<0.15	0.17, 0.31, 1.61, 0.36	−26.2	−22.8	...	−47.1, −38.7, −31.9, −23.5	100124
58	AH Oph	0.10	0.24	<0.06	0.47	54.2	52.2	...	51.7	100122(0.28)
60	V2296 Oph	0.89	0.34	<0.06	0.13	25.1	25.2	...	26.0	100119(0.44)
62	OH358.23+0.11	0.75	0.49	<0.09	4.02, 4.17, 2.04, 0.76	−8.4	−7.1	...	−13.2, −9.4, −7.7, 1.5	100124
64	WY Her	0.55	0.92	<0.06	0.94	5.1	5.6	...	3.5	100116(0.24)
66	IRC−10395	2.24	2.82	<0.11	0.13, 0.36, 0.24	20.2	19.6	...	18.7, 22.2, 27.5	100126
72	V2090 Oph	0.88	0.35	<0.06	0.27	−30.4	−29.7	...	−21.9	100122
74	UY Sct	1.63	0.22	<0.09	0.44, 0.32, 1.66, 0.35	31.3	28.9	...	22.4, 26.2, 30.4, 34.6	100126
76	V2571 Oph	0.30	<0.08	<0.07	0.25	−38.0	...	...	−38.9	100125
78	OH24.7−0.1	0.37	0.41	<0.07	0.13, 0.12, 0.13	91.6	91.6	...	70.3, 77.1, 83.4	100126
80	IRC+00364	0.77	0.67	<0.08	2.68, 2.95, 2.34, 2.77	55.6	56.1	...	44.6, 50.4, 59.7, 62.3	100124
81	V3952 Sgr	0.53	1.04	<0.05	0.17	−4.1	0.6	...	−2.1	100126(0.95)
85	EU Aql	0.20	0.11	<0.06	0.15	75.9	74.0	...	75.7	100117(0.19)
89	OH43.8+0.5	0.15	0.28	<0.08	0.12	9.3	8.2	...	−3.1	100126
91	IRAS 19083+0851	0.39	0.13	<0.05	0.57, 0.87, 0.53	50.3	53.0	...	51.4, 56.4, 60.7	100130
92	IRAS 19087+0323	0.23	0.39	<0.05	0.18	20.5	20.6	...	34.9	100130
93	RU Lyr	0.30	0.18	<0.06	0.06	15.7	15.1	...	14.9	091207(0.23)
97	IRAS 19186+0315	0.33	0.24	<0.06	0.12, 0.06	−23.9	−23.7	...	−34.2, −13.2	100130
98	YZ Dra	0.26	0.55	...	0.31	12.9	16.7	...	13.3	091206(0.66)
99	IRAS 19229+1708	0.42	0.15	<0.07	0.10, 0.16, 0.38, 0.09	42.4	32.3	...	26.7, 32.5, 42.7, 51.1	100124
100	IRC−20563	<0.09	0.24	<0.09	2.39	...	−34.6	...	−37.5	100126
101	UV Cyg	0.28	0.09	<0.07	2.64	32.8	34.2	...	13.9	091207
		0.52	<0.05	<0.06	2.23	23.4	...	...	14.2	110122
104	V1319 Aql	0.14	0.16	<0.06	0.23	−22.8	−26.3	...	−19.9	100130
105	IRAS 19374+0550	0.92	0.47	0.15	0.15	−16.1	−16.1	−16.6	−20.6	100122
107	IRAS 19422+3506	1.31	1.27	<0.10	0.39, 0.82	−49.5	−48.6	...	−66.3, −36.0	100122
111	IRAS 19495+0835	0.67	0.29	<0.08	0.52	44.3	44.2	...	46.1	100130
113	IRAS 19522+1935	0.33	0.23	<0.09	0.19	66.7	67.0	...	49.9	100130
115	V718 Cyg	0.14	<0.08	<0.08	0.54	19.5	...	...	24.3	100122
116	V719 Cyg	0.32	<0.07	<0.06	0.68	18.4	...	...	18.1	100123
120	V557 Cyg	0.20	0.15	<0.08	0.89	51.9	54.8	...	53.1	100117
121	IRAS 20171+2732	0.14	<0.07	<0.07	0.08	46.4	...	...	56.4	100123
125	V2319 Cyg	0.14	<0.06	<0.06	0.10	14.3	...	...	14.0	100116
126	IRAS 20403+3700	0.83	0.49	<0.06	0.30	−51.0	−50.2	...	−58.6	100116

Table 3
(Continued)

No.	Source	T_A^*(peak) (K)				V_{LSR}(peak) (km s^{-1})				Date(Phase)
		^{28}SiO		^{29}SiO	H_2O	^{28}SiO		^{29}SiO	H_2O	(yymmdd)
		$v = 1$	$v = 2$	$v = 0$		$v = 1$	$v = 2$	$v = 0$		
(1)	(2)	(3)	(4)	(5)	(6)	(7)	(8)	(9)	(10)	(11)
129	OH83.42−0.89	1.02	0.82	0.09	0.79, 1.24	−40.7	−40.4	−40.2	−49.5, −25.5	091207
133	IRAS 21120+0736	0.90	0.68	<0.05	0.06, 0.04	28.8	28.6	...	22.6, 34.2	100125
134	IRAS 21174+1747	0.09	<0.06	<0.05	0.11	−74.1	...	...	−78.1	091208
		0.13	0.15	<0.08	0.10	−74.0	−74.5	...	−77.6	110121
135	GH Cep	0.87	0.43	<0.09	0.28	39.3	39.4	...	36.9	091204
136	IRAS 21305+2118	0.21	0.15	<0.06	0.09, 0.12	−40.6	−40.7	...	−51.5, −28.7	091208
137	AM Cep	4.70	4.10	<0.10	0.85	−51.4	−51.1	...	−50.4	091205
140	CU Cep	1.45	0.30	<0.09	0.16	−47.6	−46.9	...	−44.0	091203(0.43)
144	V386 Cep	1.26	0.66	<0.11	1.92	−51.1	−48.6	...	−56.0	091205
147	RY And	1.62	1.89	<0.07	0.14	−1.7	−1.9	...	0.1	091205(0.50)
150	PZ Cas	0.13	<0.08	<0.07	3.15	−42.9	...	...	−41.9	091203

optical phase was obtained from the optical data provided by the American Association of Variable Star Observers (AAVSO) and the All Sky Automated Survey (ASAS) of Pojmanski (2002). Those with no regular variabilities and no available data in period remain blank. In Table 4, the integrated antenna temperature, the mean velocity, and the date of observations are given as those in Table 3. Tables 5 and 6 summarize the observational results of SiO-only maser detected sources. All columns are the same as those in Tables 3 and 4, and for the undetected maser lines, we quote the upper limit. Table 7 gives the results of H_2O-only detected sources. Columns 1–6 and 10 are the same as those in Tables 3 and 4. Columns 7–9 give the LSR radial velocity of the peak emission, the integrated antenna temperature, and the mean velocity of the detected H_2O maser line, respectively. In Table 8, we give the results of both SiO and H_2O maser undetected sources. In Columns 3–6, the upper limit is quoted as less than 3σ rms noise level.

Figure 1 shows all of the spectra from 111 detected sources, including the spectra of five sources observed at two epochs. The spectra are arranged in the same order as in Table 2. The intensity is given in units of the antenna temperature T_A^* (K) and the abscissa is V_{LSR} (km s^{-1}). For each spectrum, the identification number, the source name, molecules, and its transitions, date of observation, and optical phase are given. The peaks of H_2O maser emission from many SiO and H_2O maser sources appear around those of SiO maser emission as mentioned in Papers I and II. In the SiO detected sources, only the SiO $v = 2$ maser was detected from three stars: No. 54, V438 Oph; No. 87, OH43.9+1.2; and No. 100, IRC−20563, which was discussed in Section 4 of Paper II. From two stars, No. 91, IRAS 19083+0851, and No. 101, UV Cyg, the SiO maser emission shows double peaks.

We can also see that the peak of the H_2O maser emission is different from that of the SiO maser for many SiO/H_2O maser detected sources. They can be classified as one-way, double, and multiple peaks of the H_2O maser line profile, as described below and listed in Table 9. The others not classified as the above three types show the usual simple peak line profile of H_2O maser emission around the stellar velocity and/or the peak of SiO maser emission.

1. Five sources show a one-way peaked H_2O emission, which is blueshifted or redshifted with respect to the peak of SiO maser emission. However, these sources should be monitored at multi-epochs because another peak can be detected at another epoch. These five sources are No. 78, OH24.7−0.1; No. 89, OH43.8+0.5; No. 92, IRAS 19087+0323; No. 113, IRAS 19522+1935; and No. 126, IRAS 20403+3700.
2. Eight sources show a double-peaked H_2O emission. The double-peaked emission could have originated from the approaching and receding parts of the expanding circumstellar shell or a bipolar outflow. These facts must be confirmed by high resolution observations. They are No. 24, OZ Gem; No. 97, IRAS 19186+0315; No. 101, UV Cyg; No. 107, IRAS 19422+3506; et al.
3. Six sources show a multi-peaked H_2O emission. This emission consists of more than four peaks with different velocities. They are No. 40, AY Vir; No. 57, IRAS 17187−3750; No. 62, OH358.23+0.11; No. 74, UY Sct; No. 80, IRC+00364; and No. 99, IRAS 19229+1708. In the case of No. 40, AY Vir, the H_2O maser emission showed double peaks on 2009 June 15 (090615) but it showed multi-peaks on 2011 January 20 (110120).

The characteristics of a few individual sources can be described as follows.

AY Vir (= IRC+00237 = IRAS 13492−0325, No. 40). This star is an M6 semi-regular variable with a period of 113 days (Benson et al. 1990) and a relatively bright *IRAS* source with $F_{12} = 46.6$ Jy. Two epoch observations were performed, as shown in Figure 1 and Table 7. Only the H_2O maser emission was detected at $V_{LSR} = -45.9$ and -35.0 km s^{-1} on June 15 2009 as double peaks, while it was detected at $V_{LSR} = -44.9$, -39.4, and -34.7 km s^{-1} on 2011 January 20 as triple peaks. Takaba et al. (2001) detected H_2O masers at $V_{LSR} = -42.4$ km s^{-1} as a single peak. The SiO maser was not detected in our observations, as well as in Takaba et al. (1994)'s observations.

V445 Sct (= OH17.7−2.0 = IRAS 18276−1431, No. 77). This source is located in "RI" of Region V which has been suggested by Sevenster (2002) as a less massive post-AGB star region. Stars in this region are distinguished by their non-variability and are called "non-variable OH/IR stars" with no large-amplitude variations (Engels & Jiménez-Esteban 2007). Its spectral type is K1–K4 with $T_{eff} \sim 4200$ K (Le Bertre 1987). This fact can be explained by its evolution having ended the AGB stage and moved to the planetary nebula stage. The SiO $v = 1$ maser emission was detected at $V_{LSR} = 66.1$ km s^{-1} for the first time. The peak velocity of the SiO maser was

Table 4
Integrated Intensities and Mean Velocities of Both SiO-($J = 1$–0) and H_2O-detected Sources

No.	Source	$\int T_A^* dv$ (K km s^{-1})				V_{LSR}(mean) (km s^{-1})				Date(Phase)
		^{28}SiO		^{29}SiO	H_2O	^{28}SiO		^{29}SiO	H_2O	(yymmdd)
		$v = 1$	$v = 2$	$v = 0$		$v = 1$	$v = 2$	$v = 0$		
(1)	(2)	(3)	(4)	(5)	(6)	(7)	(8)	(9)	(10)	(11)
13	IR Per	0.59	0.90	0.02	...	−23.0	−27.9	−27.9	...	091203
		0.69	0.32	...	0.30	−24.7	−25.6	...	−18.5	110120
15	BD Eri	3.44	1.42	...	0.55	−9.1	−8.8	...	−9.6	091202(0.99)
16	RW Lep	1.03	2.31	...	1.34	−58.4	−58.8	...	−60.3	100111
17	LO Aur	3.10	2.22	...	0.50	0.6	1.3	...	4.7	090615(0.71)
22	IRC+70074	1.58	3.86	...	0.36	10.5	9.9	...	9.3	090615
23	TT Mon	0.22	...	...	0.64	39.5	...	...	42.9	091113(0.55)
24	OZ Gem	9.32	9.29	...	1.77	5.3	4.9	...	6.8	090716
25	SS Pup	4.02	4.40	...	1.40	82.5	81.3	...	84.3	091113(0.99)
28	V Leo	1.28	...	...	2.16	−27.8	...	...	−27.1	090610(0.93)
35	U CVn	1.11	...	...	0.50	−26.8	...	...	−22.9	091113(0.72)
36	T Com	3.06	2.16	...	0.18	28.4	28.9	...	27.7	091110(0.78)
41	TW Cen	0.92	0.53	0.10	0.43	−0.8	−1.2	0.2	3.8	091111(0.80)
42	R Boo	1.16	0.24	...	0.16	−45.2	−44.4	...	−42.7	091110(0.47)
46	SW Lib	0.71	0.63	...	0.33	−22.7	−19.7	...	−18.4	100116(0.56)
51	R Dra	1.75	1.25	...	0.82	−118.7	−114.5	...	−121.2	091110(0.11)
53	TU Sco	1.63	1.01	...	0.39	−14.1	−14.1	...	−13.0	100117(0.73)
54	V438 Oph	...	0.25	...	0.36	...	9.7	...	5.7	091110
55	UY Oph	1.26	1.42	...	0.18	−64.8	−63.1	...	−64.1	100119(0.43)
56	RV Ser	1.43	1.26	...	2.08	3.3	4.5	...	1.9	100124(0.47)
57	IRAS 17187−3750	14.19	3.62	...	3.32	−25.1	−24.3	...	−32.2	100124
58	AH Oph	0.67	0.64	...	0.65	51.6	53.1	...	51.7	100122(0.28)
60	V2296 Oph	1.97	1.08	...	0.25	25.9	26.6	...	26.3	100119(0.44)
62	OH358.23+0.11	5.86	2.23	...	15.34	−8.9	−9.1	...	−9.1	100124
64	WY Her	1.99	2.31	...	1.81	3.4	5.3	...	2.9	100116(0.24)
66	IRC−10395	6.52	6.38	...	1.15	20.2	20.3	...	23.7	100126
72	V2090 Oph	3.94	1.33	...	0.62	−28.4	−30.0	...	−23.9	100122
74	UY Sct	15.63	0.72	...	3.23	32.7	28.6	...	30.1	100126
76	V2571 Oph	0.90	...	...	0.39	−38.0	...	...	−38.6	100125
78	OH24.7−0.1	1.28	1.65	...	0.85	91.1	90.8	...	77.3	100126
80	IRC+00364	4.08	2.99	...	21.52	57.2	57.3	...	52.0	100124
81	V3952 Sgr	2.97	2.85	...	0.18	−0.6	0.6	...	−2.1	100126(0.95)
85	EU Aql	0.96	0.41	...	0.13	74.3	76.3	...	75.8	100117(0.19)
89	OH43.8+0.5	0.24	1.13	...	0.22	9.1	9.0	...	−3.2	100126
91	IRAS 19083+0851	2.79	0.73	...	2.87	54.2	57.3	...	56.5	100130
92	IRAS 19087+0323	0.60	1.03	...	0.32	21.1	21.1	...	34.9	100130
93	RU Lyr	0.53	0.63	...	0.21	15.1	13.8	...	14.9	091207(0.23)
97	IRAS 19186+0315	0.99	0.71	...	0.37	−23.3	−22.5	...	−31.8	100130
98	YZ Dra	1.00	1.09	...	0.38	14.8	16.5	...	13.7	091206(0.66)
99	IRAS 19229+1708	2.13	1.04	...	1.40	39.9	34.0	...	37.7	100124
100	IRC−20563	...	0.67	...	2.67	...	−34.2	...	−37.5	100126
101	UV Cyg	2.59	0.35	...	3.36	22.5	33.9	...	15.0	091207
		1.83	...	...	5.18	22.6	...	...	15.0	110122
104	V1319 Aql	0.87	0.57	...	0.70	−21.4	−23.3	...	−22.7	100130
105	IRAS 19374+0550	2.14	1.48	0.14	0.25	−16.0	−14.8	−16.8	−20.4	100122
107	IRAS 19422+3506	5.16	4.66	...	5.04	−49.0	−48.6	...	−42.9	100122
111	IRAS 19495+0835	2.40	0.62	...	1.67	46.0	43.5	...	48.0	100130
113	IRAS 19522+1935	0.89	0.59	...	0.26	67.0	67.3	...	50.0	100130
115	V718 Cyg	1.42	...	...	1.32	23.7	...	...	22.8	100122
116	V719 Cyg	2.02	...	...	1.01	19.3	...	...	18.8	100123
120	V557 Cyg	0.70	0.14	...	1.36	56.6	54.8	...	53.0	100117
121	IRAS 20171+2732	0.39	...	...	0.27	47.7	...	...	56.5	100123
125	V2319 Cyg	0.33	...	...	0.06	15.0	...	...	14.0	100116
126	IRAS 20403+3700	2.61	2.05	...	1.16	−51.5	−50.8	...	−59.5	100116
129	OH83.42−0.89	5.10	3.69	0.15	7.16	−41.0	−40.1	−40.3	−35.6	091207
133	IRAS 21120+0736	1.98	1.54	...	0.21	28.2	28.4	...	29.2	100125
134	IRAS 21174+1747	0.14	...	...	0.20	−73.9	...	...	−77.6	091208
		0.35	0.37	...	0.28	−74.0	−74.9	...	−75.5	110121
135	GH Cep	4.02	2.17	...	0.55	39.0	41.5	...	36.5	091204
136	IRAS 21305+2118	0.30	0.29	...	0.55	−40.5	−40.6	...	−43.1	091208
137	AM Cep	13.35	9.95	...	1.41	−51.0	−50.8	...	−50.3	091205
140	CU Cep	8.73	1.56	...	0.84	−46.5	−45.8	...	−46.2	091203(0.43)
144	V386 Cep	9.28	3.19	...	6.31	−51.1	−51.0	...	−53.8	091205
147	RY And	3.32	4.03	...	0.20	−2.1	−1.9	...	0.0	091205(0.50)
150	PZ Cas	0.52	...	...	4.28	−41.0	...	...	−41.8	091203

Table 5
Peak Antenna Temperatures and Velocities of SiO-only Detected Sources without H_2O

No.	Source	T_A^*(peak) (K)				V_{LSR}(peak) (km s^{-1})			Date(Phase)
		^{28}SiO		^{29}SiO	H_2O	^{28}SiO		^{29}SiO	(yymmdd)
		$v=1$	$v=2$	$v=0$		$v=1$	$v=2$	$v=0$	
(1)	(2)	(3)	(4)	(5)	(6)	(7)	(8)	(9)	(10)
2	TY Cas	1.39	0.72	...	<0.11	−58.7	−58.1	...	091112(0.12)
3	V656 Cas	2.22	2.98	...	<0.22	10.4	10.1	...	090617
7	IO Per	0.65	0.14	...	<0.10	−30.9	−34.2	...	091112
21	FX Mon	0.13	<0.10	...	<0.11	37.4	...	...	091113(0.84)
26	SV Pup	0.31	0.11	<0.12	<0.11	31.6	30.8	...	091110(0.98)
44	MW Ser	0.57	0.33	...	<0.08	44.3	43.9	...	091106
45	WW Ser	0.69	0.69	...	<0.07	22.3	21.7	...	091106(0.64)
52	RX Oph	0.35	0.25	<0.08	<0.04	−50.4	−50.1	...	100112(0.68)
59	IRAS 17230+0113	0.27	0.19	<0.06	<0.07	−22.6	−23.2	...	100121
61	MW Her	3.90	2.74	<0.11	<0.08	−50.7	−51.1	...	100118(0.21)
63	IRAS 17528+1144	0.12	<0.05	<0.06	<0.05	91.1	...	...	100123
65	IRC+10346	0.09	<0.09	<0.05	<0.05	11.0	...	...	100124
69	IRAS 18139−1811	0.56	0.42	<0.06	<0.05	43.4	43.9	...	100125
73	IRAS 18231+0855	0.08	0.08	<0.05	<0.03	−8.1	−7.6	...	100125
77	V445 Sct	0.12	<0.08	<0.08	<0.06	66.1	...	...	100125
82	OH40.1+2.4	0.27	0.31	<0.07	<0.07	48.1	47.8	...	100121
83	IRAS 18549+0905	0.33	0.21	<0.06	<0.05	18.4	18.3	...	100124
84	IRAS 18556+0811	0.40	0.22	<0.07	<0.05	37.0	35.1	...	100124
86	IRAS 18567+0003	0.15	0.09	<0.06	<0.06	48.3	48.4	...	100130
87	OH43.9+1.2	<0.08	0.09	<0.07	<0.04	...	49.3	...	100125
88	IRAS 19061+1041	0.14	0.08	<0.07	<0.04	40.3	38.8	...	100123
96	IRAS 19161+2343	0.22	0.28	<0.07	<0.06	29.1	29.1	...	100116
102	IRAS 19303+1553	0.12	0.09	<0.06	<0.05	8.0	7.0	...	100129
106	IRAS 19387+1527	0.23	0.21	<0.07	<0.05	61.7	61.3	...	100129
112	IRAS 19499+2141	0.48	0.33	<0.09	<0.07	1.6	1.7	...	100130
117	IRAS 20097+1107	0.12	<0.07	<0.08	<0.08	−15.8	...	...	100130
151	V657 Cas	3.62	2.46	...	<0.06	−14.6	−14.4	...	091206

redshifted compared to the stellar radial velocity of V_{LSR} = 61.4 km s^{-1} determined from OH and CO measurements (Herman et al. 1985; Heske et al. 1990). The H_2O maser search was negative in our observations. However, H_2O maser emission was detected by Nyman et al. (1986) and Likkel (1989). Engels (2002) performed monitoring observations and found that the H_2O maser emission became increasingly weaker and finally disappeared after 1990. The H_2O maser has a velocity range of ΔV = 9.0 km s^{-1} from 55.6 to 64.6 km s^{-1}. OH masers have been detected at V_{LSR} = 46.4 and 75.1 km s^{-1} as double peaks (Engels & Jiménez-Esteban 2007).

OH24.7−0.1 (= IRAS 18340−0720, No. 78). We identified this OH/IR star as having one-way and blueshifted triple peaks of H_2O maser emission in our observations. The peak velocities of the H_2O maser emission are 70.3, 77.1, and 83.4 km s^{-1}, which are blueshifted with respect to those of SiO v = 1 and 2 masers (V_{LSR} = 91.6 km s^{-1}). Takaba et al. (2001) detected the H_2O maser emission at V_{LSR} = 73.1 km s^{-1}. In addition, OH masers were detected at V_{LSR} = 60.3 and 110.8 km s^{-1} (Engels & Jiménez-Esteban 2007). Time monitoring observations are required for this star.

IRAS 19075+0921 (No. 90). Meixner et al. (1999) and Kohoutek (2001) classified this source as a PPN candidate. Alksnis et al. (2001) assigned it as a carbon star. The OH masers were detected at V_{LSR} = 5.3 and 19.3 km s^{-1} by Le Squeren et al. (1992) and gave the stellar velocity of 12.3 km s^{-1} (Table 2). However, Volk et al. (1993) detected CO (J = 2–1) emission centered at V_{LSR} = 38.2 km s^{-1}, which is largely redshifted from the stellar velocity of 12.3 km s^{-1}. They estimated the mass-loss rate as 9.5 × 10^{-6} $M_\odot$ yr^{-1} kpc^{-2} by adapting the method of Knapp & Morris (1985). Takaba et al. (2001) detected the H_2O maser emission at the peak velocity of V_{LSR} = 7.6 km s^{-1}. On the other hand, two components of H_2O maser emission were detected at V_{LSR} = −66.2 and 10.7 km s^{-1} with a velocity separation of 76.9 km s^{-1}. The component of V_{LSR} = −66.2 km s^{-1} is highly blueshifted with respect to the stellar velocity of 12.3 km s^{-1}. This seems to be due to the H_2O maser emission from an another source, which is located at the same line of sight. The SiO maser was not detected in our observation, as well as in Nyman et al. (1998)'s observation.

IRAS 19134+2131 (No. 95). This H_2O maser source is one of the "water fountain" PPNe. Drastic temporal variations in the line profile of H_2O masers were observed on time scales as short as one month by Likkel et al. (1992). Using the Very Long Baseline Array, Imai et al. (2007) showed that H_2O maser emission consists of two clusters of maser features, i.e., the blueshifted maser components from V_{LSR} = −121 to −117 km s^{-1} and the red-shifted components from V_{LSR} = −23 to −10 km s^{-1}. From the spatio-kinematical structure of the H_2O masers, they identified the highly collimated flow as having a projected extent of ∼140 mas and an expansion rate of ∼1.9 mas yr^{-1}, which give a dynamic age of only ∼40 yrs. We detected the only redshifted component of H_2O maser emission at a peak velocity of V_{LSR} = −9.1 km s^{-1}. This source is currently known as the only high-velocity H_2O maser source without OH emission (Deacon et al. 2007). The derived luminosity distance of this source is about 8.4 kpc (Nakashima & Deguchi 2003).

UV Cyg (= IRC+40348 = IRAS 19296+4331, No. 101). This star is classified as a semi-regular variable with the spectral type

Table 6
Integrated Intensities and Mean Velocities of SiO-only Detected Sources without H_2O

No.	Source	$\int T_A^* dv$ (K km s^{-1})			V_{LSR}(mean) (km s^{-1})			Date(Phase)
		^{28}SiO		^{29}SiO	^{28}SiO		^{29}SiO	(yymmdd)
		$v = 1$	$v = 2$	$v = 0$	$v = 1$	$v = 2$	$v = 0$	
(1)	(2)	(3)	(4)	(5)	(6)	(8)	(9)	(10)
2	TY Cas	6.86	3.90	...	−57.2	−55.0	...	091112(0.12)
3	V656 Cas	12.37	13.68	...	13.3	13.2	...	090617
7	IO Per	3.43	0.53	...	−29.6	−31.9	...	091112
21	FX Mon	0.37	...	...	36.7	...	...	091113(0.84)
26	SV Pup	0.64	0.20	...	32.1	31.1	...	091110(0.98)
44	MW Ser	0.93	0.60	...	44.1	43.6	...	091106
45	WW Ser	3.29	2.36	...	21.6	22.5	...	091106(0.64)
52	RX Oph	0.52	0.28	...	−50.8	−50.2	...	100112(0.68)
59	IRAS 17230+0113	1.11	0.64	...	−24.9	−23.7	...	100121
61	MW Her	13.44	6.79	...	−51.5	−50.6	...	100118(0.21)
63	IRAS 17528+1144	0.14	...	...	91.0	...	...	100123
65	IRC+10346	0.13	...	...	11.1	...	...	100124
69	IRAS 18139−1811	1.20	0.83	...	43.5	43.9	...	100125
73	IRAS 18231+0855	0.21	0.11	...	−8.6	−7.9	...	100125
77	V445 Sct	0.41	...	...	66.3	...	...	100125
82	OH40.1+2.4	0.76	0.84	...	49.0	47.7	...	100121
83	IRAS 18549+0905	0.53	0.55	...	18.4	18.5	...	100124
84	IRAS 18556+0811	0.74	0.83	...	37.2	36.1	...	100124
86	IRAS 18567+0003	0.52	0.24	...	47.4	47.4	...	100130
87	OH43.9+1.2	...	0.18	...	...	49.4	...	100125
88	IRAS 19061+1041	0.48	0.37	...	39.2	38.8	...	100123
96	IRAS 19161+2343	0.59	0.60	...	29.0	29.7	...	100116
102	IRAS 19303+1553	0.41	0.39	...	10.1	11.0	...	100129
106	IRAS 19387+1527	0.48	0.46	...	62.2	61.6	...	100129
112	IRAS 19499+2141	1.72	0.87	...	3.0	3.2	...	100130
117	IRAS 20097+1107	0.42	...	...	−14.9	...	...	100130
151	V657 Cas	16.65	11.42	...	−14.0	−12.7	...	091206

Table 7
Results of H_2O-only Detected Sources without SiO

No.	Source	T_A^*(peak) (K)				V_{LSR}(peak)	$\int T_A^* dv$	V_{LSR}(mean)	Date(Phase)
		^{28}SiO		^{29}SiO	H_2O	(km s^{-1})	(K km s^{-1})	(km s^{-1})	(yymmdd)
		$v = 1$	$v = 2$	$v = 0$					
(1)	(2)	(3)	(4)	(5)	(6)	(7)	(8)	(9)	(10)
4	YY Ari	<0.11	<0.09	...	0.24	−48.8	0.06	−48.9	091112
9	ET Eri	<0.09	<0.10	...	1.07	−5.0	1.37	−5.0	091114
20	IRAS 06319−0501	<0.08	<0.10	...	0.70	−60.3	0.81	−60.4	091114
27	V429 Hya	<0.15	<0.13	<0.10	0.82	4.5	1.27	4.9	091110
29	AF Leo	<0.10	<0.09	...	2.05	8.6	2.95	8.7	091105
32	S Crt	<0.18	<0.22	...	3.98, 4.02	34.9, 40.0	13.81	37.9	090615
33	SV Vir	<0.37	<0.33	...	0.61	−2.4	0.43	−2.4	090615(0.40)
38	V CVn	<0.08	<0.07	...	0.09	0.6	0.08	0.7	091114(0.10)
40	AY Vir	<0.16	<0.17	...	0.21, 0.18	−45.9, −35.0	1.22	−40.9	090615
		<0.07	<0.07	<0.07	0.28, 0.60, 0.35	−44.9, −39.4, −34.7	2.04	−41.2	110120
43	IRC−20285	<0.09	<0.11	<0.09	0.37	−2.0	1.06	−3.1	091111
48	RZ Sco	<0.11	<0.07	<0.09	0.07	−163.5	0.16	−163.5	100116(0.82)
		<0.13	<0.09	<0.09	0.13	−163.2	0.22	−163.4	110122(0.11)
67	OH10.4+0.04	<0.09	<0.08	<0.07	0.26	71.2	0.37	70.8	100124
68	IRC+30330	<0.06	<0.09	<0.09	0.13	−3.9	0.67	−6.3	100116
75	IRC−10425	<0.06	<0.06	<0.08	0.19	35.4	0.96	42.3	100126
90	IRAS 19075+0921	<0.07	<0.07	<0.08	0.08, 0.09	−66.2, 10.7	0.48	−19.7	100130
94	IRAS 19110+1045	<0.06	<0.08	<0.08	0.94	58.8	3.25	60.6	100117
95	IRAS 19134+2131	<0.07	<0.08	<0.06	0.17	−9.1	0.26	−9.1	100121
119	AC Cyg	<0.06	<0.06	...	0.06	−31.0	0.11	−30.8	091206
124	V778 Cyg	<0.09	<0.07	<0.09	2.29	−16.4	2.31	−16.5	091204
127	V Aqr	<0.07	<0.07	<0.07	0.07, 0.12	−46.2, −27.1	0.34	−30.3	100131
146	EU And	<0.10	<0.07	<0.08	1.98	−33.8	2.20	−34.1	091205
149	IRC+10537	<0.08	<0.08	...	0.22	−19.2	0.48	−18.8	091206

Table 8
Results of Both SiO ($J = 1$–0) and H_2O Undetected Sources

No.	Source	T_A^*(peak) (K)				rms (K)				Date(Phase)
		^{28}SiO		^{29}SiO	H_2O	^{28}SiO		^{29}SiO	H_2O	(yymmdd)
		$v = 1$	$v = 2$	$v = 0$		$v = 1$	$v = 2$	$v = 0$		
(1)	(2)	(3)	(4)	(5)	(6)	(7)	(8)	(9)	(10)	(11)
1	V641 Cas	<0.09	<0.09	...	<0.06	0.03	0.03	...	0.02	091114
5	RU Ari	<0.12	<0.10	...	<0.06	0.04	0.04	...	0.02	091114(0.76)
6	UZ Ari	<0.13	<0.15	...	<0.09	0.05	0.05	...	0.03	091114
8	GH Per	<0.12	<0.11	...	<0.10	0.04	0.04	...	0.04	091112
10	IRAS 03385+5927	<0.21	<0.20	...	<0.16	0.07	0.07	...	0.06	090617
11	TZ Tau	<0.09	<0.09	<0.08	<0.08	0.03	0.03	0.03	0.03	091202(0.01)
12	V394 Per	<0.12	<0.12	...	<0.06	0.04	0.04	...	0.02	091114
14	V729 Tau	<0.09	<0.08	<0.08	<0.08	0.03	0.03	0.03	0.03	091202
18	V1307 Ori	<0.10	<0.09	...	<0.08	0.04	0.04	...	0.03	091112
19	S Lep	<0.18	<0.15	...	<0.11	0.06	0.05	...	0.04	091114(0.30)
30	AZ UMa	<0.09	<0.09	...	<0.07	0.03	0.03	...	0.03	091105
31	II Hya	<0.28	<0.29	...	<0.29	0.10	0.11	...	0.10	090615
34	Y UMa	<0.09	<0.08	...	<0.09	0.03	0.03	...	0.03	091105(0.24)
37	IRC−10278	<0.21	<0.21	...	<0.15	0.07	0.07	...	0.05	090615
39	T UMi	<0.21	<0.20	...	<0.15	0.07	0.07	...	0.05	090615
47	X Her	<0.08	<0.12	...	<0.11	0.03	0.04	...	0.04	091106
49	S Sco	<0.09	<0.09	<0.08	<0.06	0.03	0.03	0.03	0.02	100117(0.48)
50	RY CrB	<0.08	<0.08	...	<0.09	0.03	0.03	...	0.03	091106
70	IRAS 18156−0653	<0.08	<0.09	<0.09	<0.06	0.03	0.03	0.03	0.02	100122
71	TU Lyr	<0.06	<0.06	<0.06	<0.06	0.02	0.02	0.02	0.02	100118
79	IRAS 18375+0510	<0.08	<0.09	<0.09	<0.06	0.03	0.03	0.03	0.02	100124
103	V1965 Cyg	<0.08	<0.08	<0.09	<0.06	0.03	0.03	0.03	0.02	100125
108	IRAS 19456+1927	<0.06	<0.07	<0.06	<0.05	0.02	0.03	0.02	0.02	100123
109	IRAS 19455+0920	<0.09	<0.06	<0.06	<0.06	0.03	0.02	0.02	0.02	100122
110	OH59.2−1.8	<0.09	<0.09	<0.09	<0.08	0.03	0.03	0.03	0.03	100124
114	IRAS 19566+3423	<0.08	<0.06	<0.06	<0.06	0.03	0.02	0.02	0.02	100122
118	IRC−10530	<0.06	<0.06	<0.06	<0.05	0.02	0.02	0.02	0.02	100213
122	IRAS 20246+2813	<0.13	<0.12	<0.12	<0.09	0.05	0.04	0.04	0.03	100119
123	IRAS 20311+4222	<0.08	<0.09	<0.09	<0.06	0.03	0.03	0.03	0.02	100117
128	IRAS 20482+3325	<0.12	<0.10	<0.12	<0.09	0.04	0.04	0.04	0.03	100119
130	U Equ	<0.09	<0.09	<0.09	<0.06	0.03	0.03	0.03	0.02	100124
131	V1899 Cyg	<0.09	<0.09	<0.09	<0.08	0.03	0.03	0.03	0.03	091204
132	RX Aqr	<0.06	<0.07	<0.06	<0.05	0.02	0.03	0.02	0.02	100213
138	TW Peg	<0.09	<0.09	<0.09	<0.05	0.03	0.03	0.03	0.02	091205
139	IRC+60342	<0.09	<0.08	<0.09	<0.06	0.03	0.03	0.03	0.02	091203
141	V384 Cep	<0.09	<0.09	<0.09	<0.09	0.03	0.03	0.03	0.03	091204
142	IRC+50434	<0.09	<0.08	<0.09	<0.06	0.03	0.03	0.03	0.02	091205
143	MP Peg	<0.09	<0.09	...	<0.06	0.03	0.03	...	0.02	091206
145	LL Peg	<0.09	<0.09	...	<0.06	0.03	0.03	...	0.02	091206
148	IRAS 23279+5336	<0.08	<0.08	<0.09	<0.06	0.03	0.03	0.03	0.02	091204
152	RS And	<0.06	<0.06	<0.06	<0.05	0.02	0.02	0.02	0.02	091207

of M6–M8. Its optical variability has a small amplitude from ∼9.9 to 10.5 m_v and the possible period is about 135.5 days from the General Catalogue of Variable Stars (GCVS) of Samus et al. (2011). Takaba et al. (2001) and Valdettaro et al. (2001) detected the H_2O maser emission as double peaks that centered at the velocity of $V_{LSR} = 18.2$ km s^{-1}. Szymczak & Engels (1995) detected double peaks of H_2O maser emission at two epochs. By their observations, the H_2O masers peaked at $V_{LSR} =$ 11.6 and 25.4 km s^{-1} with a velocity range of 16.8 km s^{-1} at one epoch (1992 December) and at $V_{LSR} = 12.7$ and 25.3 km s^{-1} with that of 15.2 km s^{-1} at another epoch (1993 April), respectively. In our observations, on December 7 2009 the H_2O maser was detected at $V_{LSR} = 13.9$ and 25.6 km s^{-1} as double peaks and SiO $v = 1$ maser also showed double peaks at $V_{LSR} = 16.6$ and 32.8 km s^{-1}, while SiO $v = 2$ maser showed a single peak at $V_{LSR} = 34.2$ km s^{-1}. On 2011 January 22 the H_2O maser was detected at $V_{LSR} = 14.2$ and 24.9 km s^{-1}, while SiO $v = 1$ maser showed a single peak at $V_{LSR} = 23.4$ km s^{-1} and SiO $v = 2$ maser was not detected.

4. RELATIVE INTENSITIES AND FULL WIDTHS AT ZERO POWER BETWEEN H_2O AND SiO MASERS

In Figures 2 and 3, we show the histograms of the number of stars according to the peak and integrated antenna temperature ratios between H_2O and SiO $v = 1$ maser lines for 28 Mira variables and 18 OH/IR stars, which are both H_2O and SiO maser detected sources. As shown in Figure 2, more than half of Mira variables are distributed in the ratios between 0 and 0.5, which means a much stronger SiO maser intensity compared to the H_2O maser. On the other hand, more than half of OH/IR stars are distributed in ratios between 0.5 and 1.0, as shown in Figure 3. These distributions show that the relative intensity ratios of H_2O to the SiO maser, in OH/IR stars are larger

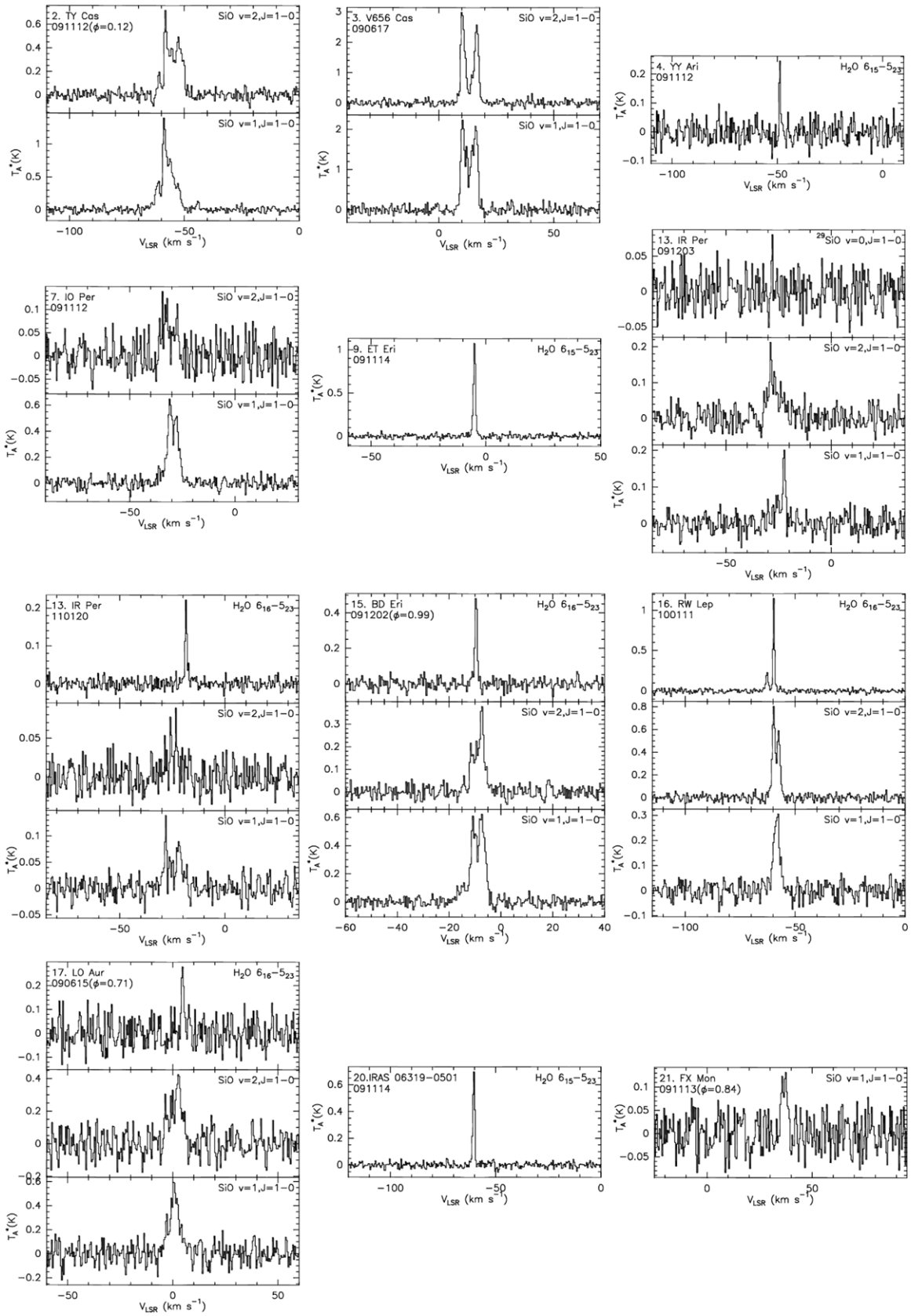

Figure 1. H_2O and SiO maser spectra of 111 stars simultaneously obtained in the H_2O $6_{16} - 5_{23}$ and SiO $v = 1, 2$, $J = 1$–0, ^{29}SiO $v = 0$, $J = 1$–0 transitions from 2009 June to 2011 January. Spectra are arranged in the same order as in the tables and indicated by the identification number. Intensity is given in units of antenna temperature T_A^* (K) and the abscissa is V_{LSR} (km s^{-1}). The identification number, the source name, the molecule and its transitions, the date of observation, and optical phase are also given in the spectrum of each source.

(An extended version of this figure is available in the online journal.)

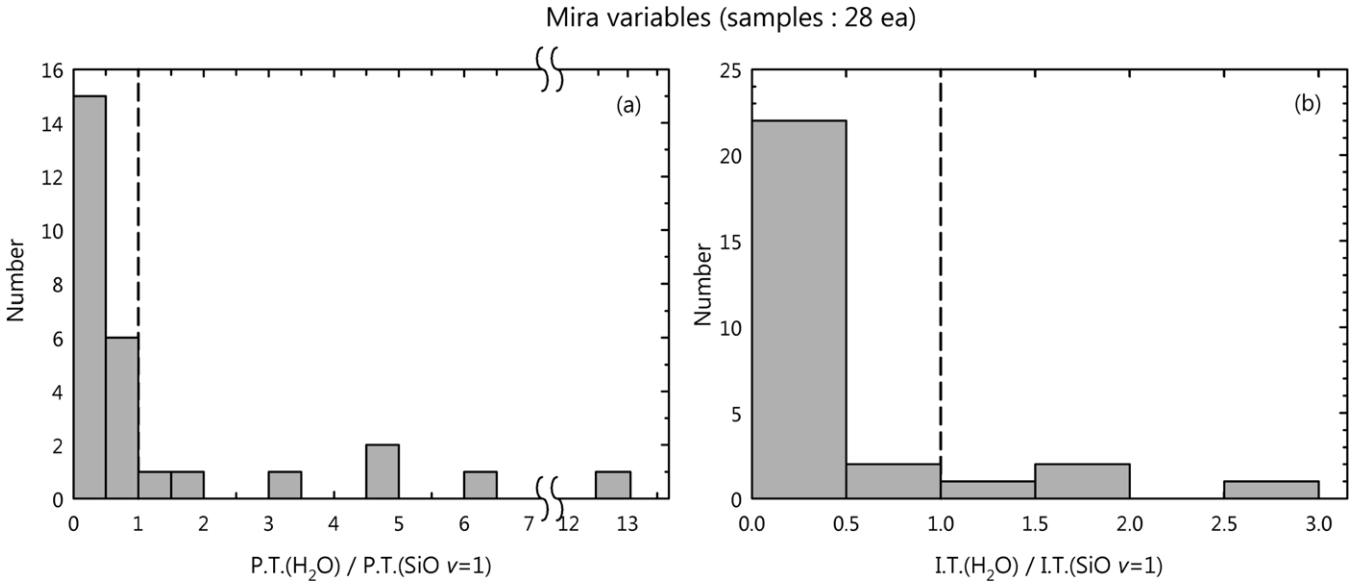

Figure 2. Distributions of (a) the peak (P.T.) and (b) integrated (I.T.) antenna temperature ratios of the H_2O to SiO $v = 1$ maser lines for Mira variables.

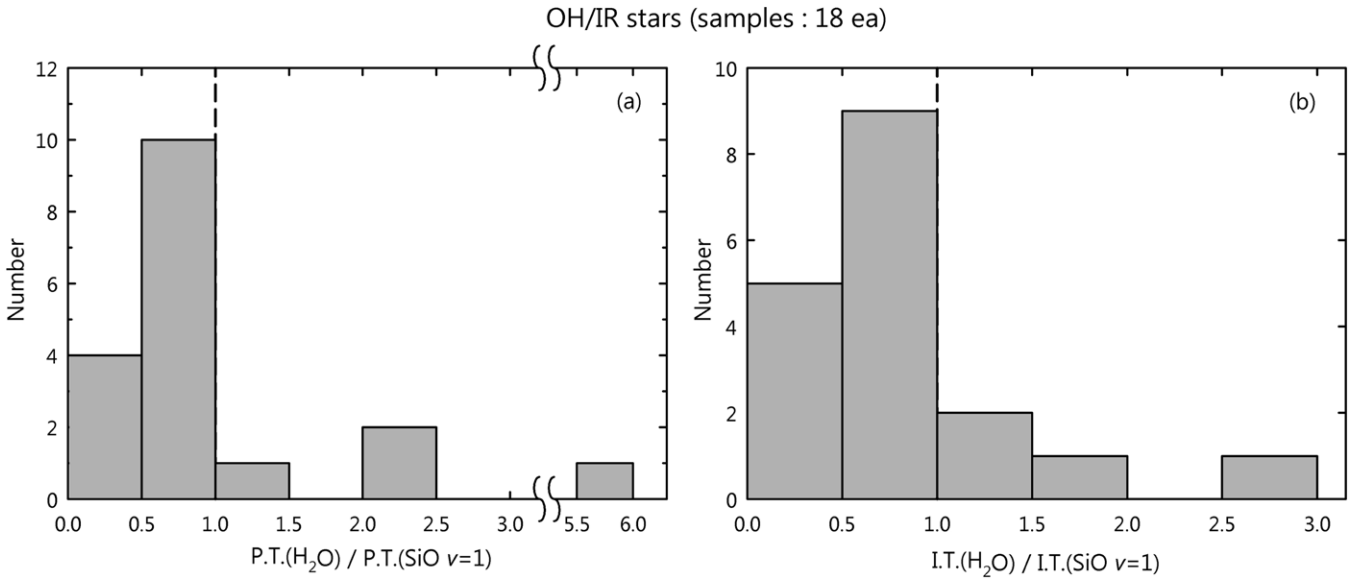

Figure 3. Distributions of (a) the peak (P.T.) and (b) integrated (I.T.) antenna temperature ratios of the H_2O to SiO $v = 1$ maser lines for OH/IR stars.

than those in Mira variables, although the intensities of the H_2O maser emission are weaker than those of the SiO masers in both OH/IR stars and Mira variables. It may be the case that the H_2O maser photon luminosities of OH/IR stars are larger than those of Mira variables and/or the SiO maser photon luminosities of OH/IR stars are smaller than those of Mira variables. Nyman et al. (1993) reported that the SiO ($v = 1$, $J = 1$–0) maser photon luminosities of OH/IR stars are similar to, but slightly smaller than, the range of photon luminosities in Mira variables. Nyman et al. (1986) suggested that the SiO masers may become collisionally quenched in OH/IR stars with a large mass-loss rate and are very weak. In addition, the peak antenna temperature ratios between the H_2O and SiO masers of Mira variables show a large spread to 13 compared to those of OH/IR stars and their average values are large compared to the average values of OH/IR stars, as shown in Table 10. We will investigate and discuss these ratios between the H_2O and SiO masers in Paper IV based on Paper I–III sample stars.

The distribution of the full width at zero power (FWZP) ratios between H_2O and SiO $v = 1$ maser lines are presented as a histogram in Figure 4. As shown in Figure 4, the FWZPs of H_2O masers are narrower than those of SiO masers for most of the Mira variables, while they are broader than those of SiO masers for most of the OH/IR stars. Table 11 gives the SiO and H_2O FWZPs and ratios for Mira variables and OH/IR stars, which were detected in both SiO and H_2O masers. The average ratios of the FWZPs of H_2O masers to those of SiO are 0.68 for Mira variables and 2.18 for OH/IR stars, respectively. These differences between the Mira variables and OH/IR stars may have originated from the different mass-loss rates and the different location of two masers. The 22 GHz H_2O masers came from above dust forming layers and we can trace the expansion velocity connected to the mass-loss rates, while SiO masers occur inside dust forming layers that are an expansion and infalling motions influenced by direct stellar pulsation (Diamond et al. 1994; Diamond & Kemball 2003). The

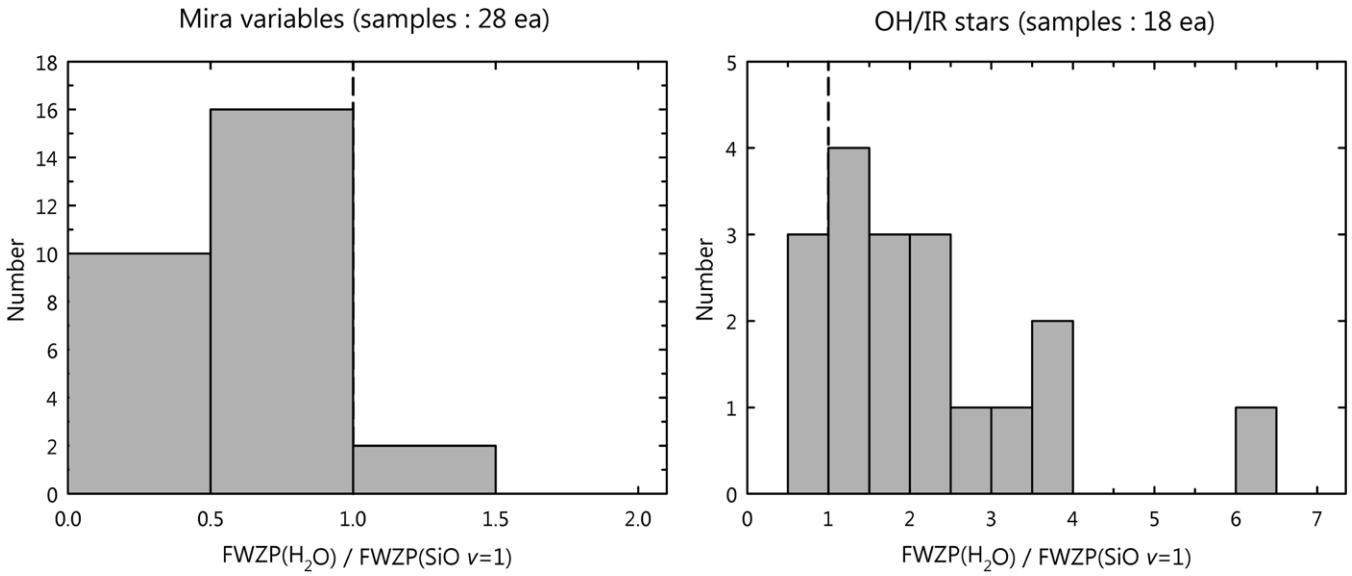

Figure 4. Number of sources as a function of the full width at zero power (FWZP) ratios of the H_2O to SiO $v = 1$ maser lines for Mira variables and OH/IR stars, respectively.

Table 9
Type of H_2O Line Profile

No.	Source	Type
24	OZ Gem	D
40	AY Vir	M
57	IRAS 17187−3750	M
62	OH358.23+0.11	M
74	UY Sct	M
78	OH24.7−0.1	OW(B)
80	IRC+00364	M
89	OH43.8+0.5	OW(B)
92	IRAS 19087+0323	OW(R)
97	IRAS 19186+0315	D
99	IRAS 19229+1708	M
101	UV Cyg	D
107	IRAS 19422+3506	D
113	IRAS 19522+1935	OW(B)
126	IRAS 20403+3700	OW(B)
127	V Aqr	D
129	OH83.42−0.89	D
133	IRAS 21120+0736	D
136	IRAS 21305+2118	D

Notes. "OW," "D," and "M" indicate one-way peaks, double peaks, and multiple peaks of the H_2O spectra, respectively. "B" and "R" in the one-way peak indicate blueshifted and redshifted with respect to stellar velocity.

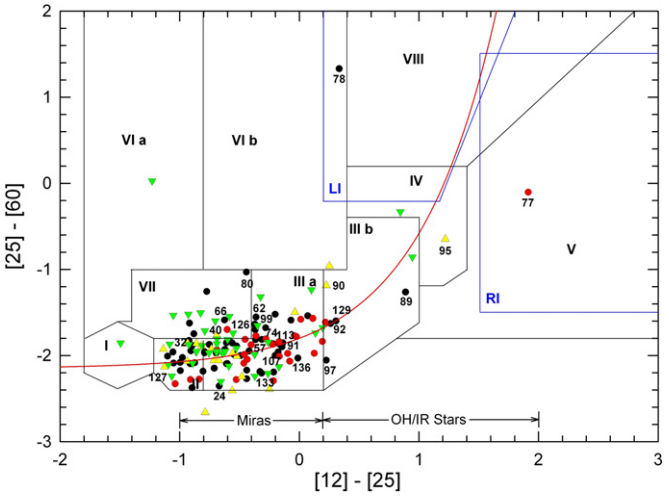

Figure 5. *IRAS* two-color diagram with the position of the observed sources in our simultaneous observations of the SiO and H_2O masers. The red line is the evolutionary track for AGB stars defined by van der Veen & Habing (1988). The black circles indicate both the SiO and H_2O maser detected sources, and the red circles and the yellow triangles indicate the SiO-only detected sources and the H_2O-only detected sources, respectively. Both SiO and H_2O maser undetected sources are marked with green inverted triangles. The sources with one-way, double, and multiple peaks of the H_2O maser are identified by their identification numbers.

OH/IR stars show higher mass-loss rates than Mira variables with a very extended circumstellar envelope. Relations between these FWZPs and mass-loss rates will also be investigated in Paper IV based on Paper I–III sample stars.

5. *IRAS* TWO-COLOR DIAGRAM OF SiO AND H_2O OBSERVED SOURCES

The *IRAS* two-color diagram for our observed sources are shown in Figure 5 by using the IRAS Point Source Catalog v2.1 (http://irsa.ipac.caltech.edu/cgi-bin/Gator/nph-dd). The two infrared colors are defined as [12]–[25] = 2.5 log (S_{25}/S_{12}) and [25]–[60] = 2.5 log (S_{60}/S_{25}), respectively. Both SiO and H_2O maser detected sources are indicated by black circles, and SiO-only detected sources without H_2O maser detections and H_2O-only detected sources without SiO maser detections are indicated by red circles and yellow triangles, respectively. Both undetected sources are marked with the inverted triangles. The red line indicates the evolutionary track for AGB stars defined by van der Veen & Habing (1988). The regions of two groups of post-AGB stars, "LI" (left of *IRAS*) and "RI" (right of *IRAS*), are denoted as blue-line areas (Sevenster 2002). Most of our observed sources are found mainly in Regions II and IIIa. In addition, a large number of H_2O-only maser detectected sources are distributed in Region II and the front part of Region IIIa, while a large number of SiO-only detected sources are distributed in the rear part of Region IIIa. However, it is difficult to discuss evolutionary sequences because of limited sample sources. As

Table 10
Averaged Peak and Integrated Antenna Temperature Ratios

Type of Object	Sample Sources	$\frac{\text{P.T.(SiO,v=2)}}{\text{P.T.(SiO,v=1)}}$	$\frac{\text{I.T.(SiO,v=2)}}{\text{I.T.(SiO,v=1)}}$	Sample Sources	$\frac{\text{P.T.(H}_2\text{O)}}{\text{P.T.(SiO,v=1)}}$	$\frac{\text{I.T.(H}_2\text{O)}}{\text{I.T.(SiO,v=1)}}$
Mira variable	33	0.90	0.78	28	1.54	0.53
OH/IR star	27	0.83	0.94	18	1.08	0.85
Semi-regular variable	6	0.87	0.79	8	3.26	1.01

Table 11
FWZP Ratios between H_2O and SiO Masers for Mira Variables and OH/IR Stars

Mira Variable	FWZP(SiO)	FWZP(H_2O)	$\frac{\text{FWZP(H}_2\text{O)}}{\text{FWZP(SiO)}}$	OH/IR Star	FWZP(SiO)	FWZP(H_2O)	$\frac{\text{FWZP(H}_2\text{O)}}{\text{FWZP(SiO)}}$
BD Eri	15.13	5.87	0.39	OH358.23+0.11	24.77	25.35	1.02
LO Aur	16.51	7.20	0.44	OH24.7−0.1	13.73	53.64	3.91
IRC+70074	13.61	9.98	0.73	OH43.8+0.5	10.33	31.14	3.01
TT Mon	9.98	7.98	0.80	IRAS 19083+0851	23.77	23.24	0.98
OZ Gem	16.90	23.94	1.42	IRAS 19087+0323	12.27	34.62	2.82
SS Pup	9.47	13.88	1.47	IRAS 19186+0315	13.47	31.96	2.37
V Leo	22.16	8.82	0.40	IRAS 19229+1708	25.82	41.16	1.59
U CVn	10.44	7.10	0.68	IRAS 19422+3506	21.22	40.81	1.92
T Com	15.17	9.47	0.62	IRAS 19495+0835	16.14	16.03	0.99
TW Cen	13.77	4.41	0.32	IRAS 19522+1935	12.27	43.53	3.55
R Boo	14.85	6.78	0.46	V719 Cyg	27.00	16.31	0.60
SW Lib	15.71	7.53	0.48	IRAS 20171+2732	14.91	19.37	1.30
R Dra	15.60	7.31	0.47	V2319 Cyg	11.30	11.30	1.00
TU Sco	7.54	5.96	0.79	IRAS 20403+3700	13.13	31.24	2.38
UY Oph	21.15	10.57	0.50	OH83.42−0.89	20.54	38.03	1.85
RV Ser	14.31	6.13	0.43	IRAS 21120+0736	11.50	25.00	2.17
AH Oph	23.12	5.16	0.22	IRAS 21174+1747	11.25	15.41	1.37
V2296 Oph	10.87	10.65	0.98	IRAS 21305+2118	6.46	41.08	6.36
WY Her	8.28	8.07	0.97				
V3952 Sgr	15.71	9.25	0.59				
EU Aql	14.20	9.68	0.68				
RU Lyr	10.11	9.68	0.96				
YZ Dra	16.25	6.35	0.39				
V557 Cyg	14.85	8.93	0.60				
GH Cep	14.79	12.21	0.83				
AM Cep	12.68	11.39	0.90				
CU Cep	27.97	22.25	0.80				
RY And	12.16	9.68	0.80				

a post-AGB Region RI source, No. 77, V445 Sct, showed the characteristics of a preplanetary nebula, as described in individual stars of the previous section. The Region IV sources, No. 95. IRAS 19134+2131, is a famous "water fountain" source, which is also described in the individual stars from the previous section. We examined the distribution of the sources with one-way, double, and multiple peaks of H_2O maser lines in the *IRAS* two-color diagram as described in Paper I. These one-way, double, and multiple peaks of H_2O maser lines can be associated with asymmetric wind and bipolar outflows, which are commonly seen in PPNe and PNe. Almost all the sources in Region IIIb, No. 89, No. 92, No. 97, No. 129 show one-way or double peaks of H_2O maser lines although the total number of observed sources are limited. This tendency is similar to the distributions of one-way or double peaks sources, as shown in Paper I, implying the development of bipolar outflows from the late stage evolution of AGB stars.

6. SUMMARY

1. For 152 evolved stars, which are known to be stellar H_2O maser sources, we detected both SiO and H_2O maser emission from 62 stars at a detection rate of 40.8%. Only SiO maser emission without H_2O maser detection was detected from 27 sources, while the H_2O-only maser emission was detected from 22 sources. The total detection rate of SiO maser was 58.6%, which included 70 new detections, while that of the H_2O maser was 55.3%. According to the type of evolved star, both SiO and H_2O masers were detected from 28 out of 47 Mira variables (60%), while they were detected from 18 sources (44%) for 41 OH/IR stars. In the case of semi-regular variables, eight of the 28 surveyed sources emitted both SiO and H_2O masers (29%).
2. Five sources showed a one-way peaked H_2O emission. Velocities of these sources appeared to be blueshifted or redshifted with respect to the SiO maser peak and the stellar velocity. Eight sources showed double peaked H_2O emission. Six sources exhibited multiple peaked H_2O emission, which consisted of more than four peaks. These multiple peaks indicated that the maser emission comes from expanding circumstellar gas where remarkable fluctuations in the velocity and/or pump rate exist.
3. The peak and integrated antenna temperature ratios of the H_2O and SiO maser lines were distributed for 28 Mira variables and 18 OH/IR stars, which are both H_2O and SiO maser detected sources. In both Mira variables and OH/IR stars, the peak and integrated antenna temperatures

of SiO masers are stronger than those of H_2O masers and the relative intensity ratios of H_2O to SiO maser in OH/IR stars are larger than those in Mira variables. The average values of the H_2O peak and integrated intensity ratio, with respect to SiO maser in Mira variables, are 1.54 and 0.53, while those in OH/IR stars are 1.08 and 0.85, respectively.

4. For both H_2O and SiO maser detected sources in Mira variables and OH/IR stars, the FWZPs of H_2O masers were narrower than those of SiO masers for Mira variables. In contrast, the FWZPs of H_2O masers were broader than those of SiO masers for OH/IR stars. The average FWZP ratios of H_2O masers to SiO masers were 0.68 and 2.18 for Mira variables and OH/IR stars, respectively. This may be due to the higher mass-loss rate of OH/IR stars with a very extended circumstellar envelope compared to Mira variables.
5. Almost all the sources in Region IIIb show one-way or double peaks of H_2O maser lines. This tendency is similar to the distributions of one-way or double peak sources, as shown in Paper I, which shows the development of bipolar outflows according to the late stage evolution of AGB stars.

This work was supported by the Basic Research Program (2011–2012) and partially supported by the "KASI–Yonsei Joint Research Program (2011–2012) for the Frontiers of Astronomy and Space Science" funded by the Korea Astronomy and Space Science Institute. In this research, we have used information from the AAVSO International Database that operates at AAVSO Headquarters, 25 Birch Street, Cambridge, MA 02138, USA and SIMBAD database that operates at CDS, Strasbourg, France.

REFERENCES

Alksnis, A., Balklavs, A., Dzervitis, U., et al. 2001, BaltA, 10, 1
Balister, M., Batchelor, R. A., Haynes, R. F., et al. 1977, MNRAS, 180, 415
Barbier-Brossat, M., Petit, M., & Figon, P. 1994, A&AS, 108, 603
Benson, P. J., & Little-Marenin, I. R. 1989, BAAS, 21, 1118
Benson, P. J., & Little-Marenin, I. R. 1996, ApJS, 106, 579
Benson, P. J., Little-Marenin, I. R., Woods, T. C., et al. 1990, ApJS, 74, 911
Bowers, P. F., & Hagen, W. 1984, ApJ, 285, 637
Brand, J., Gesaroni, R., Caselli, P., et al. 1994, A&AS, 103, 541
Bujarrabal, V. 1994, A&A, 285, 953
Bujarrabal, V., Planesas, P., & del Romero, A. 1987, A&A, 175, 164
Chen, P. S., Szczerba, R., Kwok, S., & Volk, K. 2001, A&A, 368, 1006
Cho, S.-H., Kaifu, N., & Ukita, N. 1996, A&AS, 115, 117
Cho, S.-H., & Kim, J. 2012, AJ, 144, 129 (Paper II)
Choi, Y. K., Hirota, T., Honma, M., & Kobayashi, H. 2008, in Proc. IAU Symp. 248, A Giant Step: from Milli- to Micro-arcsecond Astrometry, ed. W. J. Jin, I. Platais, & M. A. C. Perryman (Cambridge: Cambridge Univ. Press), 192
Comoretto, G., Palagi, F., Cesaroni, R., et al. 1990, A&AS, 84, 179
Cooke, B., & Elitzur, M. 1985, ApJ, 295, 175
Crocker, D. A., & Hagen, W. 1983, A&AS, 54, 405
Deacon, R. M., Chapman, J. M., Green, A. J., & Sevenster, M. N. 2007, ApJ, 658, 1096
Deguchi, S., Fujii, T., Ita, Y., et al. 2007, PASJ, 59, 559
Deguchi, S., Nakada, Y., & Forster, J. R. 1989, MNRAS, 239, 825
Deguchi, S., Sakamoto, T., & Hasegawa, T. 2012, PASJ, 64, 4
Deguchi, S., Shimoikura, T., & Koike, K. 2010, PASJ, 62, 525
Diamond, P. J., & Kemball, A. J. 2003, ApJ, 599, 1372
Diamond, P. J., Kemball, A. J., Junor, W., et al. 1994, ApJL, 430, 61
Dickinson, D. F. 1976, ApJS, 30, 259
Dickinson, D. F., Bechis, K. P., & Barrett, A. H. 1973, ApJ, 180, 831
Dickinson, D. F., & Dinger, A. S. C. 1982, ApJ, 254, 136
Doel, R. C., Gray, M. D., Humphreys, E. M. L., Braithwaite, M. F., & Field, D. 1995, A&A, 302, 797
Engels, D. 2002, A&A, 388, 252
Engels, D., Habing, H. J., Olnon, F. M., Schmid-Burgk, J., & Walmsley, C. M. 1984, A&A, 140, L9
Engels, D., & Jiménez-Esteban, F. 2007, A&A, 475, 941
Engels, D., Schmid-Burgk, J., & Walmsley, C. M. 1986, A&A, 167, 129
Engels, D., Schmid-Burgk, J., & Walmsley, C. M. 1988, A&A, 191, 283
Famaey, B., Jorissen, A., Luri, X., et al. 2005, A&A, 430, 165
Feast, M. W., & Whitelock, P. A. 2000, MNRAS, 317, 460
Groenewegen, M. A. T., Sevenster, M., Spoon, H. W. W., & Pérez, I. 2002, A&A, 390, 511
Habing, H. J. 1996, A&ARv, 7, 97
Hall, P. J., Allen, D. A., Troup, E. R., Wark, R. M., & Wright, A. E. 1990a, MNRAS, 243, 480
Hall, P. J., Wright, A. E., Troup, E. R., Wark, R. M., & Allen, D. A. 1990b, MNRAS, 247, 549
Han, F., Mao, R. Q., Lu, J., et al. 1998, A&AS, 127, 181
Han, S.-T., Lee, J.-W., Kang, J., et al. 2008, IJIMW, 29, 69
Herman, J., Baud, B., Habing, H. J., & Winnberg, A. 1985, A&A, 143, 122
Heske, A., Forveille, T., Omont, A., van der Veen, W. E. C. J., & Habing, H. J. 1990, A&A, 239, 173
Imai, H., Sahai, R., & Morris, M. 2007, ApJ, 669, 424
Imai, H., Shibata, K. M., Marvel, K. B., et al. 2003, ApJ, 590, 460
Ita, Y., Deguchi, S., Fujii, T., et al. 2001, A&A, 376, 112
Jewell, P. R., Batrla, W., Walmsley, C. M., & Wilson, T. L. 1984, A&A, 130, L1
Kim, J., Cho, S.-H., Oh, C. S., & Byun, D.-Y. 2010, ApJS, 188, 209 (Paper I)
Kleinmann, S. G., Dickinson, D. F., & Sargent, D. G. 1978, AJ, 83, 1206
Knapp, G. R., & Morris, M. 1985, ApJ, 292, 640
Kohoutek, L. 2001, A&A, 378, 843
Le Bertre, T. 1987, A&A, 180, 160
Lee, S.-S., Byun, D.-Y., Oh, C. S., et al. 2011, PASP, 123, 1398
Le Squeren, A. M., Sivagnanam, P., Dennefeld, M., & David, P. 1992, A&A, 254, 133
Lewis, B. M. 1989, ApJ, 338, 234
Lewis, B. M., & Engels, D. 1988, Natur, 332, 49
Likkel, L. 1989, ApJ, 344, 350
Likkel, L., Morris, M., & Maddalena, R. J. 1992, A&A, 256, 581
Lockett, P., & Elitzur, M. 1992, ApJ, 399, 704
Meixner, M., Ueta, T., Dayal, A., et al. 1999, ApJS, 122, 221
Nakada, Y., Izumiura, H., Onaka, T., et al. 1987, ApJL, 323, 77
Nakashima, J., & Deguchi, S. 2003, PASJ, 55, 229
Nyman, L.-Å., Hall, P. J., & Le Bertre, T. 1993, A&A, 280, 551
Nyman, L.-Å., Hall, P. J., & Olofsson, H. 1998, A&AS, 127, 185
Nyman, L.-Å., Johansson, L. E. B., & Booth, R. S. 1986, A&A, 160, 352
Pojmanski, G. 2002, AcA, 52, 397
Samus, N. N., Durlevich, O. V., Kazarovets, E. V., et al. 2011, General Catalog of Variable Stars (Moscow: Sternberg Astronomical Inst.)
Schwartz, P. R., & Buhl, D. 1975, ApJL, 201, 27
Sevenster, M. N. 2002, AJ, 123, 2788
Shintani, M., Imai, H., Ando, K., et al. 2008, PASJ, 60, 1077
Spencer, J. H., Winnberg, A., Olnon, F. M., et al. 1981, AJ, 86, 392
Szymczak, M., & Engels, D. 1995, A&A, 296, 727
Takaba, H., Iwata, T., Miyaji, T., & Deguchi, S. 2001, PASJ, 53, 517
Takaba, H., Ukita, N., Miyaji, T., & Miyoshi, M. 1994, PASJ, 46, 629
Valdettaro, R., Palla, F., Brand, J., et al. 2001, A&A, 368, 845
van der Veen, W. E. C. J., & Habing, H. J. 1988, A&A, 194, 125
Volk, K., Kwok, S., & Woodsworth, A. W. 1993, ApJ, 402, 292
Wilson, R. E. 1953, General Catalogue of Stellar Radial Velocities (Washington, DC: Carnegie Inst. Publ. 601)
Winnberg, A., Engels, D., Brand, J., Baldacci, L., & Walmsley, C. M. 2008, A&A, 482, 831
Zuckerman, B. 1979, ApJ, 230, 442
Zuckerman, B., & Lo, K. Y. 1987, A&A, 173, 263